

# *Differences between the 2018 and 2019 stratospheric polar vortex split events*

Article

Accepted Version

Butler, A. H., Lawrence, Z. D., Lee, S. H., Lillo, S. P. and Long, C. S. (2020) Differences between the 2018 and 2019 stratospheric polar vortex split events. *Quarterly Journal of the Royal Meteorological Society*, 146 (732). pp. 3503-3521. ISSN 1477-870X doi: 10.1002/qj.3858 Available at <https://centaur.reading.ac.uk/91388/>

It is advisable to refer to the publisher's version if you intend to cite from the work. See [Guidance on citing](#).

Published version at: <http://dx.doi.org/10.1002/qj.3858>

To link to this article DOI: <http://dx.doi.org/10.1002/qj.3858>

Publisher: Royal Meteorological Society

All outputs in CentAUR are protected by Intellectual Property Rights law, including copyright law. Copyright and IPR is retained by the creators or other copyright holders. Terms and conditions for use of this material are defined in the [End User Agreement](#).

[www.reading.ac.uk/centaur](http://www.reading.ac.uk/centaur)

**CentAUR**

Central Archive at the University of Reading

Reading's research outputs online

---

1 **ORIGINAL ARTICLE**

2 Quarterly Journal of the Royal Meteorological Society

3 **Differences between the 2018 and 2019**  
4 **stratospheric polar vortex split events**

5 **Amy H. Butler<sup>1\*</sup> | Zachary D. Lawrence<sup>2,3\*</sup> | Simon H. Lee<sup>4\*</sup> | Samuel P. Lillo<sup>2,3\*</sup> | Craig S. Long<sup>5\*</sup>**

<sup>1</sup>NOAA Chemical Sciences Laboratory, 325 Broadway, Boulder, Colorado 80305

<sup>2</sup>Cooperative Institute for Research in Environmental Sciences (CIRES), University of Colorado, Boulder, Colorado 80309

<sup>3</sup>NOAA Physical Sciences Laboratory, 325 Broadway, Boulder, Colorado 80305

<sup>4</sup>Department of Meteorology, University of Reading, Reading, UK, RG6 6BB

<sup>5</sup>NOAA National Centers for Environmental Prediction (NCEP) Climate Prediction Center, 5830 University Research Drive, College Park, Maryland 20740

**Correspondence**

Amy H. Butler, CIRES and NOAA CSL, Boulder, CO, 80305, USA  
Email: amy.butler@noaa.gov

**Funding information**

Natural Environment Research Council, Grant/Award Number: NE/L002566/1.

Two recent occurrences in February 2018 and January 2019 of a dynamic split in the Northern Hemisphere stratospheric polar vortex are compared in terms of their evolution and predictability. The 2018 split vortex was associated with primarily wavenumber-2 wave forcing that was not well predicted more than 7-10 days ahead of time, and was followed by persistent coupling to the surface with strong weather impacts. In 2019 the vortex was first displaced by slow wavenumber-1 amplification into the stratosphere, which was predictable at longer lead times, and then split; the surface impacts following the event were weaker. Here we examine the role of large-scale climate influences, such as the phase of the El Niño-Southern Oscillation, the Quasi-biennial Oscillation and Madden-Julian Oscillation, on the wave forcing, surface impacts, and predictability of these two events. Linkages between the forecast error in the stratospheric polar vortex winds with the forecast error in the Quasi-biennial Oscillation and Madden-Julian Oscillation are examined.

**KEYWORDS**

polar vortex, stratosphere, teleconnections, prediction, sudden stratospheric warming, stratosphere-troposphere coupling

---

\* Equally contributing authors.

## 6 1 | INTRODUCTION

7 Disruptions of the wintertime Northern Hemisphere (NH) stratospheric polar vortex, marked by rapidly warming  
8 temperatures and a reversal of the zonal-mean zonal winds from westerly to easterly, occur on average about every  
9 other year (Butler et al., 2017). These so-called “sudden stratospheric warmings” (SSWs) involve the displacement of  
10 the vortex off the pole, the split of the vortex into two vortices, or some combination of the two (Charlton and Polvani,  
11 2007). These dramatic events 10-50 km above the Arctic are increasingly recognized as being potential sources of  
12 sub-seasonal to seasonal (S2S) predictability of wintertime weather (e.g., Butler et al., 2019; Domeisen et al., 2020a).

13 Two recent SSWs occurred on February 12 2018 and January 2 2019 (based on the reversal of the daily-mean 10  
14 hPa 60°N zonal-mean zonal wind in ERA-Interim reanalysis). In 2018 the vortex abruptly split in two, while in 2019  
15 the vortex was first displaced and then split (Rao et al., 2019). While both disruptions eventually resulted in a split  
16 vortex, there were important differences in how they evolved, their predictability, and their ultimate influence on the  
17 troposphere in the following weeks (Karpechko et al., 2018; Rao et al., 2018, 2019, 2020). For example, while the  
18 2018 SSW was predicted at lead times of 10 days or less (Lee et al. (2019); typical for mid-winter SSWs, see Domeisen  
19 et al. (2020b)), the 2019 SSW could be predicted more than a week beyond that (Rao et al., 2020). This enhanced  
20 predictability was linked to the ability of the S2S prediction systems to largely capture planetary-scale (wavenumber  
21 1) wave driving in mid-December 2018, weeks prior to the 2019 split vortex (Rao et al., 2019).

22 Another difference in the SSWs was that while the 2018 event was followed by the canonical weather pattern  
23 associated with the negative phase of the Northern Annular Mode (NAM) for up to 2 months (Greening and Hodgson,  
24 2019), the 2019 event was followed by weaker and shorter-lived stratosphere-troposphere coupling, despite the split  
25 vortex persisting for an extended period of time (Lee and Butler, 2019). The stronger amplitude of stratospheric wind  
26 reversal in 2018 was statistically linked to increased probability of downward coupling to the surface (Rao et al., 2020).

27 The contrasting characteristics in evolution and predictability may be related to differences in large-scale circula-  
28 tion patterns during these two winters (Rao et al., 2019). For example, in 2018 the tropical Pacific was in a moderate  
29 La Niña state, while in 2019 there was a moderate El Niño. In general, poleward-propagating tropospheric planetary-  
30 scale (i.e., wavenumbers  $k=1-3$ ) “wave trains”, typically forced by tropical convective heating associated with the El  
31 Niño-Southern Oscillation (ENSO) or the Madden-Julian Oscillation (MJO), can linearly interfere with the climatologi-  
32 cal extratropical wave pattern (Domeisen et al., 2019; Garfinkel et al., 2012a). When this interference is constructive,  
33 these large-scale waves can amplify into the extratropical stratosphere, leading to a weakening of the polar vortex  
34 (Smith and Kushner, 2012; Fletcher and Kushner, 2013). These tropically-forced wave-trains can also modulate pat-  
35 terns in the extratropical troposphere that precede SSWs (Barriopedro and Calvo, 2014). These so-called precursor  
36 patterns are often different for split and displacement vortex events (Garfinkel et al., 2010; Cohen and Jones, 2011;  
37 Attard et al., 2016).

38 In the tropical stratosphere, the Quasi-biennial Oscillation (QBO) can also alter where vertically-propagating  
39 waves will break and deposit their momentum in the stratosphere. While the mechanism coupling the tropical strato-  
40 spheric winds to the polar vortex is still uncertain (Garfinkel et al., 2012b; Anstey and Shepherd, 2014; White et al.,  
41 2015), one possibility is that the QBO changes the location of the subtropical critical line, beyond which the wind is  
42 easterly and where quasi-stationary planetary scale waves cannot propagate (Charney and Drazin, 1961). This mech-  
43 anism, termed the Holton-Tan effect, leads to changes in wave momentum convergence, driving an associated mean  
44 meridional circulation that weakens the polar vortex and increases the likelihood of mid-winter SSWs during the east-  
45 erly QBO phase (Holton and Tan, 1980). Lu et al. (2020) also find evidence that the QBO is associated not only with  
46 changes in the location of wave breaking but also with changes to wave structure, with greater wavenumber-1 distur-  
47 bance of the polar vortex in the easterly QBO phase. In general, S2S prediction systems do not intrinsically simulate

48 the QBO, but are able to persist the initialized tropical stratospheric wind conditions for a couple of weeks before  
49 degrading towards model climatology (typically a weak easterly state) (Butler et al., 2016; Garfinkel et al., 2018).

50 The two split polar vortex events in February 2018 and January 2019 were preceded by conditions with differ-  
51 ent phases of the QBO and ENSO, as well as differently phased but active periods of MJO evolution. These differ-  
52 ences in the large-scale climate patterns, and how well prediction systems captured their influences on stratosphere-  
53 troposphere coupling, likely had implications for the predictability of these events. Here we describe the evolution of  
54 the two events in Section 3.1 and their differences in predictability in Section 3.2. We then quantify how errors in the  
55 QBO and MJO forecasts in particular contributed to differences in the predictability of these major SSWs in Section  
56 3.3.

## 57 2 | DATA AND METHODS

58 We use daily-mean fields from the ERA-Interim reanalysis (Dee et al., 2011) to describe the evolution of the atmo-  
59 sphere and sea surface temperatures in Section 3.1 and for forecast verification in Section 3.2-3.3. Daily anomalies  
60 were computed by removing a daily climatology calculated as the mean value of each calendar day over the 1979-2018  
61 period. The Northern Annular Mode (NAM) index was calculated at each pressure level by computing deseasonalized  
62 daily-mean geopotential heights averaged over 65-90°N with global-mean geopotential height anomalies removed  
63 (Gerber and Martineau, 2018). The resulting time series are normalized to have unit variance, and multiplied by -  
64 1 such that a negative NAM index denotes an anomalously weak polar vortex (and vice versa). The QBO index is  
65 described by the first and second time-extended empirical orthogonal functions (EOFs) of 30-day mean tropical (5°S-  
66 5°N) zonal winds in the layer from 10 hPa to 70 hPa (using ERA-40 reanalysis back to 1960 to extend the historical  
67 data). Following Fraedrich et al. (1993) and Wang et al. (1995), the time-extended matrix is built using a sliding window  
68 of fifteen 30-day periods.

69 The MJO index (the Real-time Multivariate MJO, or RMM) is calculated as in Wheeler and Hendon (2004) and is  
70 provided by the Australian Bureau of Meteorology [[http://www.bom.gov.au/climate/mjo/graphics/rmm.74toRealttime.  
71 txt](http://www.bom.gov.au/climate/mjo/graphics/rmm.74toRealttime.txt)]. Bivariate root mean square error (RMSE) of the MJO forecasts for the S2S prediction systems in Section 3.3 is  
72 calculated following Rashid et al. (2011). The amplitude of ENSO is determined from the National Centers for Environ-  
73 mental Prediction (NCEP) Climate Prediction Center Oceanic Niño Index based on ERSSTv5 sea surface temperatures  
74 [[https://origin.cpc.ncep.noaa.gov/products/analysis\\_monitoring/ensostuff/ONI\\_v5.php](https://origin.cpc.ncep.noaa.gov/products/analysis_monitoring/ensostuff/ONI_v5.php)].

75 In Section 3.2-3.3, we use real-time forecasts and hindcasts from the Subseasonal to Seasonal (S2S) project  
76 database (Vitart et al., 2017). We consider eight different prediction systems (CMA, ECCC, ECMWF, JMA, KMA,  
77 CNRM, NCEP, and UKMO). These prediction systems are all initialized at different frequencies and provide forecasts  
78 out to 4-6 weeks. They also have different reforecast periods. The details of the prediction systems used in our anal-  
79 ysis, including ensemble size, forecast length and frequency are provided in Supporting Information (Table S1 and S2).  
80 Note that JMA and ECCC do not provide a T+0h forecast; we have noted in figure captions where forecasts from  
81 these systems are shifted by 1 day relative to other systems. We bias-correct the model forecasts by subtracting the  
82 initialization date and lead-time dependent biases with respect to the ERA-Interim climatology, where the biases are  
83 determined using the full hindcast dataset available for each model. We note here limitations of this method: the bias  
84 correction method assumes that biases can be linearly removed, which may not be accurate especially during extreme  
85 vortex events; and determining the biases is dependent on the reforecast climatology which can be noisy for periods  
86 of less than 20 years.

87 We also examine moment diagnostics calculated from NCEP CFSv2 data (Saha et al., 2014) in Section 3.2 to ex-

amine the subseasonal prediction of the stratospheric vortex geometry. We specifically focus on the centroid latitude and aspect ratio diagnostics similar to that calculated in Seviour et al. (2013). We use bias-corrected 10 hPa geopotential height fields to calculate the parameters of the best-fit ellipse to the geometrical shape of the polar vortex. These calculations differ from those in Seviour et al. (2013) only in that the moments calculations are not weighted by the geopotential heights within the vortex edge contour; this is done so that the distortion of the vortex is better represented as the relative sizes and strengths of the sister vortices evolve during the split events. The centroid latitude and aspect ratio provide compact information about the degree of displacement of the vortex, and the degree of stretch in the vortex, respectively. They thus provide insight into how and when CFSv2 predicted the specific geometrical evolution of the 2018 and 2019 vortex splits. Note we also do not impose any persistence criteria to classify the events, as done in Seviour et al. (2013), but instead show the diagnostics for each day. We also use a region segmentation algorithm to confirm when the contour representing the vortex edge separates into more than one distinct region (e.g., Lawrence and Manney, 2018).

## 3 | RESULTS

### 3.1 | The evolution of the 2018 and 2019 polar vortex split events

The 2017-2018 and 2018-2019 NH stratospheric polar vortices evolved in a similar way through mid-December (Figure 1a). In the 2017-2018 winter, the vortex weakened in December, re-strengthened into the new year, weakened briefly in the latter half of January, and then rapidly decelerated and reversed on 12 February 2018 in a major SSW. The vortex split into two sister vortices, with the larger lobe ending up over central Canada and the smaller lobe over Europe (Figure 1b). The dominance of the Canadian vortex following this split event is not common; usually the Siberian vortex is dominant (Matthewman et al., 2009). The anomalous stratospheric warming peaked over the Atlantic sector within days of the zonal-mean zonal wind reversal. The zonal wind reversal following the February 2018 SSW was large in amplitude and persistent, lasting through the month and setting daily records for minimum zonal-mean zonal wind speeds at 60°N and 10 hPa for the period 1979-2019 in ERA-Interim. The vortex subsequently recovered, and the so-called “final warming” (the last reversal of the wintertime vortex to its easterly summer state) occurred on the climatological mean date of 15 April.

In the 2018-2019 winter, the vortex began to weaken in mid-December, ending with a major SSW on January 2 2019. This zonal wind reversal also set daily records for minimum zonal-mean zonal wind speeds for the 1979-2019 period, though the amplitude of the reversal was not as large as for the February 2018 event (Lee and Butler, 2019). In this case, the vortex first displaced over the North Atlantic region, warming the polar stratosphere; after the vortex split, the sister vortices ended up over Europe and eastern Canada (Figure 1c). These lobes of the disrupted vortex persisted in these locations with nearly equivalent size for three weeks after the SSW (Figure S1), and stayed split even after the zonal-mean zonal winds returned to westerly. After the SSW, the vortex radiatively recovered, then continued to intensify, leading to daily records for maximum zonal-mean zonal wind intensity in March 2019. Following this vortex strengthening, the vortex decelerated, ending in a final warming slightly later than average on 23 April (Lee and Butler, 2019).

While for both SSWs the polar vortex split, with one lobe of the vortex over Eurasia and the other over North America, both the drivers and the impacts of these events were actually quite different. Figure 2 shows the sea surface temperature (SST) and 500 hPa geopotential height anomalies in the month prior to the 2018 and 2019 vortex splits, respectively. In the winter of 2017-2018, a La Niña state prevailed (the DJF Oceanic Niño index was  $-0.9^{\circ}\text{C}$ ), with anomalously cold SSTs over the eastern and central tropical Pacific and tropical Indian Ocean. Opposite-signed tropical

128 Pacific SST anomalies emerged the following winter of 2018-2019, with El Niño conditions (the DJF Oceanic Niño  
129 index was  $+0.8^{\circ}\text{C}$ ). The pattern of 500 hPa height anomalies in the 30 days prior to the SSWs are at least partially  
130 related via teleconnections to the different tropical Pacific conditions that were present in each winter. La Niña is  
131 canonically associated with an anomalous ridge over the Aleutians and a negative Pacific-North American (PNA)-like  
132 pattern over North America, and El Niño with an anomalous Aleutian low and a positive PNA-like pattern (Deser et al.,  
133 2017).

134 The canonical La Niña teleconnection pattern was apparent in the month prior to the February 2018 SSW (Fig-  
135 ure 2a), with some differences from the composite pattern: the anomalous Aleutian ridge was shifted northwest, the  
136 anomalous western North American trough was largely absent, and the ridging over the southeastern US was shifted  
137 northward. Persistent Aleutian blocking, mostly during La Niña winters, is a tropospheric precursor to SSWs, particu-  
138 larly split vortex events (Martius et al., 2009; Castanheira and Barriopedro, 2010; Barriopedro and Calvo, 2014; Cohen  
139 and Jones, 2011; Bancalá et al., 2012). Indeed, in the month prior to the February 2018 SSW, at least three strong  
140 poleward eddy heat flux events (40-80°N, 300 hPa) occurred (Figure 3; positive or poleward meridional heat flux is a  
141 proxy for vertically propagating waves from the troposphere to stratosphere). These predominantly  $k=2$  wave pulses,  
142 associated with anomalous ridging over the Aleutians and also the Ural region (Martius et al., 2009), have been found  
143 to “precondition” the vortex, similar to other historical SSWs (Lawrence and Manney, 2020). The  $k=2$  eddy heat fluxes  
144 set 2-3 new daily record highs at 300 hPa in the month prior to the SSW (Figure 3b). The total eddy heat fluxes at  
145 300 hPa also set daily record highs around 13-14 January 2018 and in the 2-3 days prior to the SSW (Figure 3b). The  
146 daily record-breaking values of eddy heat flux at 10 hPa (Figure 3a) in the week leading up to the SSW are likely a  
147 manifestation of the amplified  $k=2$  pattern from the surface to 10 hPa as the vortex splitting occurred (Birner and  
148 Albers, 2017; White et al., 2019; de la Cámara et al., 2019).

149 The canonical El Niño teleconnection was apparent prior to the 2019 SSW as an anomalous Aleutian low, another  
150 “precursor pattern” for SSWs (Figure 2b; Garfinkel et al. (2010); Bao et al. (2017)). While there were two noticeable  
151  $k=2$  eddy heat flux events in mid-November and early December, the vortex was primarily perturbed by a substantial  
152 but relatively slow amplification of  $k=1$  eddy heat fluxes associated with the anomalous Aleutian low and Ural blocking  
153 high. The increase in  $k=1$  eddy heat flux activity began in early to mid-December (Figure 3c,d), as the polar vortex was  
154 displaced off the pole. It is interesting to note that historically El Niño SSWs are associated with more  $k=1$  amplification  
155 compared to La Niña SSWs (Barriopedro and Calvo, 2014). The  $k=1$  eddy heat fluxes at 300 hPa and 10 hPa set daily  
156 record highs in the two weeks prior to the 2019 SSW (Figure 3c,d). Finally, note that a strong  $k=3$  pulse, setting a new  
157 daily record high at 300 hPa (Figure 3d), occurred just days before the 2019 SSW (Rao et al., 2019).

158 The differences in wave activity in the 10 days before each SSW is highlighted in Figure 4. In 2018 (Figure 4a,b),  
159 the  $k=2$  pattern was nearly barotropic (vertically-stacked from the surface to the mid-stratosphere), a feature common  
160 to split vortex events (Esler and Scott, 2005; Matthewman et al., 2009). The amplitude of  $k=2$  exceeded  $k=1$  from  
161 roughly 500-30 hPa and was well above climatology from 500-1 hPa. In comparison, in 2019 (Figure 4c,d), there was a  
162 strongly baroclinic (westward tilting with height) predominantly  $k=1$  pattern. This anomalous wave pattern projected  
163 well onto the climatological wave pattern, suggesting constructive linear interference, which would allow amplification  
164 into the stratosphere (Smith and Kushner, 2012). Note also that in 2019, the amplitude of  $k=2$  was below climatology  
165 throughout the atmospheric column, while  $k=3$  was above climatology from the surface to 30 hPa and matched  $k=1$   
166 amplitudes in the troposphere (see also Figure 3d). While disruptions of the polar vortex have only rarely been linked  
167 to  $k=3$  activity (Shi et al., 2017), we think there are two potential explanations for its presence here. One possibility is  
168 that the  $k=3$  pattern manifested as anomalous Pacific, Atlantic, and Ural blocking highs (Figure 4c), in a similar manner  
169 to the  $k=2$  pattern in 2018 (Figure 4a) but with enhanced sinuosity. As the vortex displaced over the Atlantic sector,  
170 the Atlantic blocking high in particular may have helped to pull the vortex apart from below (Woollings et al., 2010,

171 Figure S1). Another possibility is that nonlinear interactions between large-scale waves and the stratospheric basic  
172 state, as the vortex first displaced off the pole and then split, introduced a substantial  $k=3$  component (Smith, 1983).

173 We also note that the downward influence following the SSW differed in 2018 and 2019. Both SSWs had a  
174 similar persistence of the zonal-mean zonal wind reversal in the stratosphere (19 days in 2018 and 21 days in 2019),  
175 though the magnitude of the reversal, which was roughly  $-24$  m/s in 2018 and only  $-10$  m/s in 2019 (Lee and Butler,  
176 2019), might have played a role in the subsequent downward coupling (Karpechko et al., 2017; Rao et al., 2020). In  
177 particular, in 2018, the developing anomalous high pressure over the polar stratosphere had a downward influence  
178 that reached the troposphere within a week (Figure 5a). The anomalously high geopotential height anomalies over  
179 the Arctic were associated with an equatorward shift of the North Atlantic storm track and a negative NAM that  
180 persisted from late February to mid-March. Significant winter storms, such as the "Beast from the East", impacted  
181 Europe in late February (Greening and Hodgson, 2019); and as the North Atlantic blocking retrograded westward  
182 over Greenland in March (Figure S1), the northeastern United States also saw much colder weather and a surge of  
183 nor'easter extratropical cyclones (<https://www.ncdc.noaa.gov/sotc/national/201803>). The stratospheric polar vortex  
184 did not reform until March.

185 In 2019, strongly positive polar cap geopotential anomalies at 10 hPa, or the negative phase of the stratospheric  
186 NAM, were observed 10-12 days prior to the zonal wind reversal (Figure 5b). In the troposphere, anomalous and  
187 retrograding North Atlantic blocking was apparent, as in 2018, but the blocking grew weaker in the weeks following  
188 the SSW rather than stronger, and the impacts from the SSW did not project strongly onto the North Atlantic Os-  
189 cillation (the regional manifestation of the NAM). Note that the NAM at 1000 hPa did change to its negative phase  
190 from mid-January to early February, despite the fact that the free troposphere was in a positive NAM state for most  
191 of that period (Figure 5b). It has been previously noted that the surface response to anomalous stratospheric forcing  
192 is amplified compared to the troposphere (Baldwin and Thompson, 2009; Domeisen et al., 2020a). Nonetheless, the  
193 stratosphere-troposphere coupling following the SSW was not particularly strong nor persistent, with few notable  
194 impacts except perhaps the tropospheric "polar vortex" event that led to record cold in the central United States in  
195 late January (which was vertically well-aligned with the lobe of the stratospheric polar vortex over central Canada),  
196 followed by a week of anomalous cold over the eastern US in early February.

197 In essence, both the upward (troposphere to stratosphere) and downward (stratosphere to troposphere) coupling  
198 were quite different for these two events. The 2018 SSW was driven by primarily  $k=2$  eddy heat fluxes associated with  
199 barotropic blocking patterns, and resulted in a persistently negative phase of the NAM and cold weather outbreaks.  
200 The 2019 SSW was preceded by slow and steady amplification of  $k=1$  that first displaced the vortex before it split,  
201 and resulted in strong downward coupling to the tropopause that only briefly translated to typical surface impacts of  
202 a SSW. It should be noted that in the historical record, split polar vortex events have been observed to follow both  $k=1$   
203 and  $k=2$  tropospheric precursor patterns (Bancalá et al., 2012), with the precursor pattern strongly tied to the phase  
204 of ENSO (Barriopedro and Calvo, 2014), in agreement with the 2018 and 2019 cases here. Additionally, irrespective  
205 of ENSO phase, both SSWs were preceded by strong anomalous ridging over the Ural mountains in northwestern  
206 Eurasia (also apparent in Figure 2 and Figure S1). Previous studies have noted the Ural blocking high as an important  
207 driver of increased upward-propagating wave activity (Garfinkel et al., 2010; Karpechko et al., 2018; Peings, 2019).

208 Other large-scale circulation patterns such as the QBO and the MJO may have influenced these two events.  
209 Figure 6a shows polar vortex weakening events at  $60^{\circ}\text{N}$  and 10 hPa plotted in the phase space of the QBO, as  
210 described by the first and second time-extended EOFs of 30-day mean tropical ( $5^{\circ}\text{S}$ - $5^{\circ}\text{N}$ ) zonal winds in the layer  
211 from 10 hPa to 70 hPa. The light gray lines trace the historical QBO values; note that the QBO amplitude does not  
212 vary much, with the obvious exception of the 2016 disruption (Coy et al., 2017). It is apparent that polar vortex  
213 weakenings tend to occur when the tropical stratospheric winds below roughly 30 hPa are easterly (i.e., below the

214 diagonal EOF1=EOF2 line; 42 events), relative to when the stratospheric winds below 30 hPa are westerly (18 events).  
215 Both the February 2018 and January 2019 SSWs occurred in the top two QBO octants for most vortex weakenings.  
216 However the February 2018 event occurred during a period when the tropical winds at 50 hPa were weakly westerly  
217 (with strong easterlies above 40 hPa), whereas in January 2019 the tropical winds at 50 hPa were easterly (with strong  
218 westerlies above 40 hPa); i.e., the QBO was roughly  $180^\circ$  out of phase between the two events. The maximum  
219 daily 100 hPa 45-75°N eddy heat flux anomaly in the 10 days prior to vortex weakening (shading of dots) generally  
220 corresponds with the magnitude of the polar vortex weakening (size of dots). There is some preference for preceding  
221 eddy heat flux anomalies to be enhanced for events occurring in phases with easterlies in the tropical stratosphere  
222 below 30 hPa (Holton and Tan, 1980; Lu et al., 2020).

223 Like ENSO, the MJO can lead to poleward-propagating wave trains that shift longitudinally depending on where  
224 the anomalous tropical convection occurs (Hoskins and Karoly, 1981). Figure 6b shows MJO-polar vortex states for  
225 February 2018 and January 2019 in a historical context. Polar vortex weakenings at 60°N and 10 hPa (dot size) and  
226 the minimum value of the 1000 hPa NAM index in the following 45 days (shading), are plotted in the phase space of  
227 the RMM index. Note that only simultaneous relationships between the MJO and polar vortex strength are indicated  
228 here; other studies have suggested there is a 10-20 day lag between the MJO tropical forcing and extratropical and  
229 stratospheric impacts (Kang and Tziperman, 2017). Many SSWs have occurred when the MJO is inactive (i.e., within  
230 the unit circle on the phase space diagram). However, for both the February 2018 and January 2019 SSW, the MJO  
231 was active in phases 5-7 prior to the events, consistent with, e.g., Garfinkel et al. (2012a) and Liu et al. (2014).

232 Specifically, 15 days before the February 2018 SSW, enhanced tropical convection was evident over the western  
233 Pacific as the MJO hit near record amplitudes in phase 6-7 (Figure 6b). This phase of the MJO is typically followed  
234 10-15 days later by enhanced extratropical eddy heat fluxes (Garfinkel et al., 2014) with polar vortex weakening  
235 (Garfinkel et al., 2012a). A week after the SSW, the MJO entered phase 8 which is associated with a negative NAO  
236 pattern (Lin et al., 2009; Henderson et al., 2016). Thus it is possible that the MJO played a significant role via its extra-  
237 tropical teleconnection in encouraging a North Atlantic blocking pattern by mid- to late February that was conducive  
238 to downward coupling from the stratosphere (Barnes et al., 2019). By early March 2018, the MJO signal in phase 2  
239 had decayed; interestingly, this is also around when the mid-troposphere showed less coupling with the stratosphere  
240 (Figure 5), though the surface NAM stayed negative through mid-March. In comparison, prior to the January 2019  
241 SSW, the MJO was entering phase 5-6. The MJO then moved quickly at low amplitude through phase 6-7, stalled in  
242 phase 8 in early January, decayed, and then re-emerged around 18 January in phases 4-5. Overall, the MJO was in a  
243 similar phase as 2018 but with weaker amplitude and faster decay to neutral state.

244 Figure 6b indicates that the MJO phase may modulate the surface response following the polar vortex deceleration  
245 (Barnes et al., 2019). There is a preference for lower minimum NAM values in the 45 days following SSWs that  
246 occur in active (RMM magnitude >1) MJO phases 6-1 compared to phases 2-5 (the frequency of events with minimum  
247 NAM  $< -2\sigma$  is 12/19 = 0.63 for phases 6-1, and 7/20 = 0.35 for phases 2-5). This suggests that the MJO enhanced  
248 the likelihood of a more negative surface NAM response following both the February 2018 and January 2019 SSWs.

### 249 3.2 | The predictability of the 2018 and 2019 polar vortex splits

250 In general, SSWs are not predictable more than 10-20 days in advance, though this can vary by individual event  
251 (Tripathi et al., 2014; Karpechko, 2018). Vortex splits are likely to be even less predictable than vortex displacements  
252 (Taguchi, 2015, 2018). The predictability of the 2018 SSW has been detailed in previous studies. Karpechko et al.  
253 (2018) found that S2S prediction systems forecast the 2018 SSW about 11 days in advance, and accurate prediction  
254 was linked to the ability of the models to correctly capture the location of anomalous Ural blocking (e.g., Figure 2). Rao

255 et al. (2018) found similar timescales of predictive skill for the 2018 event. Lee et al. (2019) found that anticyclonic  
256 Rossby wave breaking in the North Atlantic, which was tied to the amplification of the Ural blocking high and  $k=2$   
257 in the stratosphere, was not well forecast and thus limited how soon prediction systems forecast the event. For the  
258 2019 event, Rao et al. (2019) found predictive skill at up to 18 day lead times in the S2S prediction systems.

259 We use real-time forecasts of the S2S prediction systems to compare the prediction of the 2018 and 2019 vortex  
260 splits. We show the percent of ensemble members accurately detecting the first zonal-mean zonal wind reversal in the  
261 forecast within  $\pm 3$  days of the observed SSW date (Figure 7a,c), and the percent of ensemble members that detect the  
262 first zonal wind reversal in the forecast outside this 3-day window (Figure 7b,d) for different S2S prediction systems.  
263 In 2018, most prediction systems had fewer than 75% of members accurately detecting the SSW until 10-13 days  
264 prior to the SSW. Models with poor stratospheric resolution, such as CMA, had even shorter predictability of about  
265 7 days. However most of the prediction systems also showed increased probability ( $> 50\%$ ) of a "false" SSW (mostly  
266 predicted to occur near the end of January, not shown) when initialized between January 7-20, during the period of  
267 record-setting upper tropospheric wave activity (Figure 3). In other words the models may have tried to break down  
268 the vortex too soon in response to this anomalous tropospheric eddy heat flux.

269 In 2019, the detection of the SSW was possible at longer lead times, with KMA, ECMWF, and UKMO prediction  
270 systems showing accurate detection of the SSW for forecasts initialized up to 15-22 days prior. However, other  
271 systems such as NCEP showed accurate detection at shorter lead times compared to the 2018 event (though the  
272 false alarm rate peaked in NCEP just before the peak in hit rate, suggesting NCEP predicted an SSW for forecasts  
273 initialized as early as Dec 11th, but not at the correct time). Across the prediction systems, there was a gradual  
274 increase in false alarms for forecasts initialized in the weeks prior to the event, likely tied to the gradual increase of  
275  $k=1$  amplitudes (Figure 3).

276 Note here we are showing detection rates using bias-corrected forecasts. The bias-correction affects primarily  
277 extended-range forecasts; a version of Figure 7 without bias correction is available in Supplemental Information (Fig  
278 S2) for comparison. We find at forecast times of greater than 10 days significant biases that can affect accurate  
279 prediction of stratospheric variability for some prediction systems. While Figure 7 accounts for these biases, we  
280 note that in particular CMA and NCEP CFSv2 have large (opposing) biases at forecast times of greater than 10 days  
281 during parts of the winter season. For example, NCEP is biased at extended-range (10-40 days) towards a weaker-  
282 than-observed vortex, particularly in early winter (Figure S3). On the other hand, CMA is biased at extended-range  
283 towards a stronger-than-observed vortex for initializations throughout the winter.

284 Given that the February 2018 SSW was a predominantly  $k=2$  split vortex event while the January 2019 SSW first  
285 displaced by an amplifying  $k=1$  before splitting, we investigate how well the NCEP CFSv2 predicted these differences  
286 in morphology. NCEP CFSv2 forecasts of polar vortex geometry are derived from 10 hPa geopotential heights (Seviour  
287 et al., 2013). The calculation of the aspect ratio, which measures the elongation of the vortex (where larger aspect  
288 ratio means more elongation), and the centroid latitude, which designates the center latitude position of the vortex, is  
289 described in Section 2. Figure 8a,c shows the predicted vortex evolution for the February 2018 SSW. Here, individual  
290 ensemble-mean forecasts run diagonally, with increasing forecast day on the y-axis, so that forecast validation times  
291 line up in each vertical column. During the 2018 winter season, at forecast times beyond roughly 20 days, CFSv2  
292 generally predicted a tendency for the vortex to become displaced to latitudes near and below  $70^\circ\text{N}$  by early February  
293 (Figure 8a), with little elongation (Figure 8c). Only for forecasts of less than 10-14 days was NCEP able to better  
294 capture both the observed center latitude of the vortex and the elongation of the vortex. The prediction system  
295 captured the observed vortex elongation that occurred between January 20-25 for forecast times of up to 10 days,  
296 which was also when a false SSW was forecast (Figure 7b); and only accurately predicted the observed split vortex  
297 (here defined as an aspect ratio greater than 2.4) for forecast times of less than 10 days.

298 In contrast, for the 2019 SSW (Figure 8b,d), NCEP CFSv2 consistently and accurately predicted a displaced vortex  
299 to latitudes near and equatorward of 70°N by mid-December 2018 even up to 20 days in advance. However, the  
300 forecasts for the end of December into January strongly indicated the event would be a displacement, even for 5-20  
301 day forecasts, as NCEP struggled to capture the elongation and split of the vortex. The difficulty in capturing the  
302 event evolution is likely related to failure of the models to capture the  $k=3$  peak at longer forecast times (Rao et al.,  
303 2019). The observed split of the vortex, which occurred December 28 2018-January 2 2019, was only accurately  
304 reflected in the forecasts initialized at most a week ahead of time, even shorter lead times than in 2018.

305 Finally, we consider how well the large-scale surface response, as measured by the 1000 hPa NAM index for days  
306 10-30 following each SSW, was predicted by the S2S prediction systems' ensemble-mean (Figure 9). The observed  
307 NAM during this 20-day period was -1.23 standardized units following the 2018 SSW, but only -0.60 standardized  
308 units following the 2019 SSW (see Figure 5). For each SSW, we show how the forecast NAM response was verified for  
309 forecasts initialized two weeks prior to the event and then for the 10 days after the SSW occurred; gray dots indicate  
310 that the forecast value was within  $\pm 0.5$  standard deviations of the ERA-Interim response. For most prediction systems,  
311 as expected, the forecast of the surface response is better predicted for initializations closer to the 10-30 day window  
312 following each SSW (i.e., at shorter lead times).

313 Prior to the 2018 SSW (Figure 9a), most prediction systems were suggesting a NAM response that was more  
314 positive than observed (blue shading), particularly when initialized in late January, when the forecasts backed off  
315 from a SSW occurring (Figure 7a). KMA and UKMO continued to underestimate the negative NAM response even in  
316 forecasts initialized after the SSW. In 2019 (Figure 9b), again most forecasts were suggesting a more positive NAM  
317 response than observed in the forecasts initialized prior to the event, though ECMWF showed little error in verification  
318 even in forecasts initialized on December 20th (and also had greater than 70 % of members detecting the observed  
319 SSW, Figure 7c). Other prediction systems, such as UKMO and NCEP, continued to underestimate the negative NAM  
320 response until after the SSW occurred. CMA generally predicted too positive of a response prior to, and too negative  
321 of a response after, both the 2018 and 2019 SSW.

322 Note that the predicted NAM response has been bias-corrected in Figure 9. Without bias correction (Figure  
323 S4), CMA generally predicted too weak a NAM response while NCEP predicted a more negative NAM response than  
324 observed across almost all lead times in both 2018 and 2019. This is consistent with the strong vortex bias in CMA and  
325 the weak vortex bias in NCEP. The systematic bias correction thus has a substantial impact on verification following  
326 these events.

### 327 **3.3 | Linking errors in the QBO and MJO forecasts to errors in polar vortex prediction**

328 Accurate extended-range (week 2-5) forecasts of polar vortex variability in the S2S prediction systems may be linked  
329 to their ability to simulate processes and teleconnections correctly. In this section, we examine the relationship of  
330 forecast errors in the QBO and MJO to errors in the polar vortex forecast leading up to the 2018 and 2019 SSWs.  
331 Throughout this section we use bias-corrected forecasts, but the results are the same if we use uncorrected forecasts.

332 In 2018, the QBO at 50 hPa was weakly westerly. Averaging over forecast-times for 4 initializations (or launch  
333 dates) prior to the SSW that are consistent across prediction systems (Figure 10a), we can see that although the  
334 S2S prediction systems were initialized with similar tropical stratospheric wind values (with the exception of JMA and  
335 ECCC), the forecast tropical winds degrade to an easterly state at 50 hPa within 10 days for almost all systems. Models  
336 without an intrinsic QBO typically have weak climatological easterlies in the tropics (Butler et al., 2016). All systems  
337 thus show too easterly winds in the tropics at almost all forecast times; JMA and ECCC show the greatest errors at  
338 20-30 day forecast times.

339 A different situation was present in 2019, when the QBO at 50 hPa was easterly but more rapidly transitioning to  
340 neutral as westerlies descended from above (Figure 10c). The prediction systems degraded the initialized easterlies  
341 more rapidly than observed, so in this case, most of the systems had tropical winds that were too westerly compared  
342 to ERA-Interim. The one exception was NCEP which had too easterly winds at all forecast times. UKMO had the  
343 smallest errors at 10-30 day forecast times, while JMA had the largest errors at 20-30 day forecast times.

344 We examine the relationship between errors in the predicted tropical stratospheric winds for the 7-11 February  
345 2018 validation dates and errors in the stratospheric polar vortex (SPV) for the 12-16 February 2018 validation dates  
346 (Figure 10b; following Rao et al. (2019)), for different forecast initialization dates. We might expect via the Holton-Tan  
347 relationship that a more easterly QBO error would be linked to a more easterly SPV error (i.e., a positive correlation).  
348 However, at first glance it appears the opposite is true in 2018; forecasts with more easterly QBO error had too strong  
349 of polar vortex winds. Upon further examination, we see that the amplitude of the relationship across the 4 launch  
350 dates shown ( $r=-0.31$ ) is largely a reflection of the decreased error, particularly for polar vortex strength, at shorter  
351 lead-times. Only at the earliest launch date (18 January 2018, blue dots in Fig 10b) is the correlation of SPV error to  
352 QBO error significantly positive. The systems with the greatest easterly QBO error at 20-30 day forecast times, JMA  
353 and ECCO, also show the smallest (more easterly) SPV error for this launch date.

354 In 2019 (Figure 10d), because the 28 Dec-1 Jan QBO forecast error is mostly positive (i.e., the winds were too  
355 westerly compared to observed), the correlation with the 2-6 Jan SPV error is positive across all launch dates ( $r=0.38$ ).  
356 Again, the amplitude of the correlation across launch dates is a reflection of the reduced errors in the SPV at shorter  
357 lead-times. At the earliest launch date of December 6 (blue dots), the correlation is significantly positive as expected,  
358 and the systems with the more easterly QBO errors, NCEP and UKMO, also had the smallest (more easterly) SPV  
359 errors. Thus beyond 1-3 week forecast times, the biases in polar vortex winds and QBO winds may be linked as  
360 expected from the Holton-Tan relationship (Garfinkel et al., 2018).

361 Note that for individual launch dates less than 1-3 weeks prior to the SSWs, the relationship between errors in  
362 QBO and SPV is quite different for 2018 and 2019. Namely, the launch dates from 25 January-8 February 2018  
363 all show significant negative correlations, whereas the launch dates from 13-27 December 2018 show insignificant  
364 correlations and disagree in sign. This suggests that prediction systems that better predicted the QBO in the week  
365 prior to the February 2018 SSW also better predicted the SPV, while in 2019 there was little gain for systems better  
366 predicting the QBO. The negative correlations in 2018 are particularly puzzling because they suggest the systems  
367 that predicted a more easterly QBO also predicted a more westerly SPV. We think it likely that these relationships are  
368 a reflection of some systems better predicting both the QBO state and the SPV state in 2018, rather than a causal  
369 linkage between the QBO and SPV errors at shorter lead-times.

370 We also consider links between the bivariate RMSE (Rashid et al., 2011) of the MJO forecasts and the error in  
371 both the SPV and NAM forecasts (Figure 11). Since the correlation across all 4 launch dates (shown in upper right  
372 corner of each panel) is largely a measure of the change in error in both SPV/NAM and MJO RMSE with shorter lead-  
373 times, we instead focus on the correlations for each launch date separately. Considering first the relationship of MJO  
374 RMSE to the SPV error (Figure 11a,c), it is evident that in general, for most launch dates, there is little relationship  
375 between the RMSE of the predicted MJO for the week before the SSW and the error in the predicted SPV. This may be  
376 a reflection of the general underestimation of the observed MJO amplitude and slower eastward propagation in the  
377 extended range by the S2S systems (Vitart, 2017; Lim et al., 2018, see also Figure S5-S6 in Supporting Information),  
378 which may affect the MJO teleconnections and influence on the SPV. Or, it may be that we need to consider longer-  
379 lagged relationships between the MJO error and SPV error; here we have selected validation periods a week apart to  
380 maximize the number of forecasts we can compare, but relationships between MJO and SPV have been found to be  
381 largest at 10-20 day lags (Kang and Tziperman, 2017). For launch dates closer to the 2018 SSW, there is a stronger

382 positive relationship, showing models that had reduced MJO RMSE also had reduced error in the SPV forecasts, but  
383 these may not be causally linked.

384 Finally we examine the relationship of the MJO RMSE to errors in the NAM forecasts (Figure 11b,d). Here, we only  
385 consider the 4 prediction systems (CMA, ECMWF, NCEP, and UKMO) that have long enough forecasts to compare  
386 the error in NAM forecasts validated for the 22 Feb-14 Mar 2018 and 12 Jan-1 Feb 2019 periods (the same NAM  
387 forecasts shown in Figure 9) with the MJO RMSE validated the week prior to the observed SSW. Note that ECMWF  
388 will dominate these correlations because it has many more ensemble members than the other three. The overall  
389 correlation across launch dates is weak and insignificant, as the NAM error is not consistently smaller across prediction  
390 systems for shorter lead-times. In 2018, for the 29 January and 5 February launch dates, the relationship between the  
391 NAM error after the SSW and the RMSE of the MJO the week prior to the SSW is significantly negatively correlated.  
392 In particular, we note that ECMWF and UKMO both predicted too positive of 22 Feb-14 Mar NAM response for the  
393 29 January and 1 February launch dates (Figure 9), despite having low RMSE for their MJO forecast, suggesting a  
394 well-predicted MJO did not mean a better NAM forecast in 2018. Only for the 8 Feb launch date is the lower MJO  
395 RMSE linked to lower NAM error, which may suggest the MJO helped induce the negative NAM once the SSW had  
396 occurred.

397 In 2019, no significant relationship between MJO RMSE and NAM error was found for any launch date except  
398 27 December. Overall, Figure 11b,d suggests that the NAM error after the 2018 and 2019 SSW was not closely tied  
399 to the ability of the prediction systems to capture the MJO the week prior to the SSW.

## 400 4 | CONCLUSIONS

401 In this study, we performed an in-depth comparison between two split vortex events that occurred on February 12  
402 2018 and January 2 2019. There were substantial differences in the evolution of these events, their surface impacts,  
403 and their predictability. Here, we have examined how those differences may have been tied to differences in large-  
404 scale circulation patterns, such as ENSO, the MJO and the QBO, and their teleconnections.

405 The 2018 SSW was primarily a wavenumber-2 event preceded by anomalous Aleutian and Ural blocking highs,  
406 a tropospheric pattern which commonly precedes SSWs occurring in La Niña winters such as this one. However the  
407  $k=2$  forcing that ultimately split the vortex was predictable at timescales of less than 7-10 days. The 2018 SSW was  
408 followed by swift and persistent coupling to the surface, with substantial impacts on late winter weather over Europe  
409 and the eastern United States. The negative NAM response was generally under-predicted in amplitude by most  
410 prediction systems until the SSW occurred.

411 The 2019 SSW was instead a wavenumber-1 event, which first displaced the polar vortex over the North Atlantic  
412 before splitting. This SSW was preceded by an Aleutian low and a North Atlantic/Ural blocking high, which interest-  
413 ingly manifested as a strong wavenumber-3 forcing days before the vortex split. The moderate El Niño in the 2019  
414 winter likely contributed to the persistent precursor pattern that led to the amplification of  $k=1$  into the stratosphere,  
415 and ultimately to the SSW. Because this SSW was associated with a slow build-up of  $k=1$ , it was predictable at much  
416 longer lead-times, though the prediction systems only predicted the vortex would split (rather than displace) at lead  
417 times of less than a week. After this event, there was weaker coupling to the surface with only minor weather impacts.  
418 The predicted NAM response was still mostly too positive for the majority of prediction systems except for forecasts  
419 initialized after the SSW. To understand the differences in evolution and predictability on S2S timescales, we examined  
420 in particular how the QBO and MJO may have influenced these events and their impacts. While both SSWs occurred  
421 in phases of the QBO historically conducive to SSWs, the QBO was 180 degrees out of phase in 2018 and 2019. This

422 difference in QBO state played a role in the forecast biases in S2S prediction systems. Namely, in 2018 the predic-  
423 tion systems were not able to maintain the weak westerly state at 50 hPa and were biased easterly at all forecast  
424 times, while in 2019 they largely captured the easterlies at 50 hPa but weakened too fast, so were biased westerly.  
425 Nonetheless, in both years for forecasts initialized more than 3 weeks from the SSW, a Holton-Tan relationship was  
426 apparent between the error in the QBO and the error in the SPV, with more easterly errors in the QBO significantly  
427 correlated to more easterly error in the SPV. A significant positive relationship for the February 2018 SSW was also  
428 seen between the MJO RMSE and the error in the SPV for launch dates less than 2 weeks prior to the SSW, and for  
429 the error in the NAM for the launch date closest to the SSW. On the other hand, for the 2019 SSW, little significant  
430 relationships were found between the RMSE of MJO forecasts and the error in the NAM or the error in the SPV.

431 While this is only a case study of two polar vortex events, and so statistical relationships cannot be inferred or  
432 confirmed, it demonstrates the large inter-event variability of SSW impacts and predictability (Gerber and Martineau,  
433 2018). A substantial part of this variability may not be due to the morphology of the SSW itself as some studies  
434 suggest (Mitchell et al., 2013), but to other large-scale climate patterns in which the SSW evolves. While much  
435 understanding has been gained regarding why and how SSWs occur, further work remains on how we can better  
436 predict the stratosphere-troposphere coupling signal given the intrinsic variability of the large-scale circulation during  
437 any given SSW event.

## 438 Supporting Information

439 Table S1. Model versions used in the prediction analysis of the 2018 SSW.

440 Table S2. Model versions used in the prediction analysis of the 2019 SSW.

441 Figure S1. Evolution of the 10 hPa geopotential height and temperature anomalies, and 500 hPa geopotential height  
442 and surface temperature anomalies, from 21 days prior to 21 days after the 2018 and 2019 SSWs.

443 Figure S2. The non-bias-corrected version of Figure 7.

444 Figure S3. Biases in the NCEP CFSv2 prediction system.

445 Figure S4. The non-bias-corrected version of Figure 9.

446 Figure S5. MJO forecasts for 4 different launch dates prior to the February 2018 SSW.

447 Figure S6. MJO forecasts for 4 different launch dates prior to the January 2019 SSW.

## 448 Acknowledgements

449 S.H.L. acknowledges funding by the Natural Environment Research Council (NERC) via the SCENARIO Doctoral Train-  
450 ing Partnership (NE/L002566/1).

## 451 references

452 Anstey, J. A. and Shepherd, T. G. (2014) High-latitude influence of the quasi-biennial oscillation. *Quarterly Journal of the Royal*  
453 *Meteorological Society*, **140**, 1–21. URL: <http://dx.doi.org/10.1002/qj.2132>.

454 Attard, H. E., Rios-Berrios, R., Guastini, C. T. and Lang, A. L. (2016) Tropospheric and Stratospheric Precursors to the January  
455 2013 Sudden Stratospheric Warming. *Monthly Weather Review*, **144**, 1321–1339. URL: [https://doi.org/10.1175/MWR-](https://doi.org/10.1175/MWR-D-15-0175.1)  
456 [D-15-0175.1](https://doi.org/10.1175/MWR-D-15-0175.1).

457 Baldwin, M. P. and Thompson, D. W. (2009) A critical comparison of stratosphere-troposphere coupling indices. *Quarterly*  
458 *Journal of the Royal Meteorological Society*, **135**, 1661–1672. URL: <http://doi.wiley.com/10.1002/qj.479>.

- 459 Bancalá, S., Krüger, K. and Giorgetta, M. (2012) The preconditioning of major sudden stratospheric warmings. *Journal of Geo-*  
460 *physical Research: Atmospheres*, **117**, D04101. URL: [http://onlinelibrary.wiley.com/store/10.1029/2011JD016769/](http://onlinelibrary.wiley.com/store/10.1029/2011JD016769/asset/jgrd17642.pdf?v=1&t=hux7gxx1&s=a67470248062c314123c9e63c30d6064ca9eb5bd)  
461 [asset/jgrd17642.pdf?v=1&t=hux7gxx1&s=a67470248062c314123c9e63c30d6064ca9eb5bd](http://onlinelibrary.wiley.com/store/10.1029/2011JD016769/asset/jgrd17642.pdf?v=1&t=hux7gxx1&s=a67470248062c314123c9e63c30d6064ca9eb5bd).
- 462 Bao, M., Tan, X., Hartmann, D. L. and Ceppi, P. (2017) Classifying the tropospheric precursor patterns of sudden stratospheric  
463 warmings. *Geophysical Research Letters*, **44**, 8011–8016. URL: <http://dx.doi.org/10.1002/2017GL074611>.
- 464 Barnes, E. A., Samarasinghe, S. M., Ebert-Uphoff, I. and Furtado, J. C. (2019) Tropospheric and Stratospheric Causal Pathways  
465 Between the MJO and NAO. *Journal of Geophysical Research: Atmospheres*, **124**, 9356– 9371. URL: [https://doi.org/10.](https://doi.org/10.1029/2019JD031024)  
466 [1029/2019JD031024](https://doi.org/10.1029/2019JD031024).
- 467 Barriopedro, D. and Calvo, N. (2014) On the Relationship between ENSO, Stratospheric Sudden Warmings, and Blocking.  
468 *Journal of Climate*, **27**, 4704–4720. URL: <http://journals.ametsoc.org/doi/abs/10.1175/JCLI-D-13-00770.1>  
469 <http://journals.ametsoc.org/doi/pdf/10.1175/JCLI-D-13-00770.1>.
- 470 Birner, T. and Albers, J. R. (2017) Sudden Stratospheric Warmings and Anomalous Upward Wave Activity Flux. *SOLA*, **13A**,  
471 8–12.
- 472 Butler, A., Charlton-Perez, A., Domeisen, D. I. V., Garfinkel, C., Gerber, E. P., Hitchcock, P., Karpechko, A. Y., Maycock, A. C.,  
473 Sigmond, M., Simpson, I. and Son, S.-W. (2019) Chapter 11 - Sub-seasonal Predictability and the Stratosphere. In *Sub-*  
474 *Seasonal to Seasonal Prediction* (eds. A. W. Robertson and F. Vitart), 223–241. Elsevier. URL: [http://www.sciencedirect.](http://www.sciencedirect.com/science/article/pii/B9780128117149000115)  
475 [com/science/article/pii/B9780128117149000115](http://www.sciencedirect.com/science/article/pii/B9780128117149000115).
- 476 Butler, A. H., Arribas, A., Athanassiadou, M., Baehr, J., Calvo, N., Charlton-Perez, A., Déqué, M., Domeisen, D. I. V., Fröhlich,  
477 K., Hendon, H., Imada, Y., Ishii, M., Iza, M., Karpechko, A. Y., Kumar, A., MacLachlan, C., Merryfield, W. J., Müller, W. A.,  
478 O'Neill, A., Scaife, A. A., Scinocca, J., Sigmond, M., Stockdale, T. N. and Yasuda, T. (2016) The Climate-system Historical  
479 Forecast Project: Do stratosphere-resolving models make better seasonal climate predictions in boreal winter? *Quarterly*  
480 *Journal of the Royal Meteorological Society*, **142**, 1413–1427. URL: <http://dx.doi.org/10.1002/qj.2743>.
- 481 Butler, A. H., Sjöberg, J. P., Seidel, D. J. and Rosenlof, K. H. (2017) A sudden stratospheric warming compendium. *Earth System*  
482 *Science Data*, **9**, 63–76. URL: <https://www.earth-syst-sci-data.net/9/63/2017/>.
- 483 de la Cámara, A., Birner, T. and Albers, J. R. (2019) Are sudden stratospheric warmings preceded by anomalous tropospheric  
484 wave activity? *Journal of Climate*, **32**, 7173–7189. URL: <https://doi.org/10.1175/JCLI-D-19-0269.1>.
- 485 Castanheira, J. M. and Barriopedro, D. (2010) Dynamical connection between tropospheric blockings and stratospheric polar  
486 vortex. *Geophysical Research Letters*, **37**, L13809. URL: <https://doi.org/10.1029/2010GL043819>.
- 487 Charlton, A. J. and Polvani, L. M. (2007) A new look at stratospheric sudden warmings. Part I: Climatology and modeling  
488 benchmarks. *Journal of Climate*, **20**, 449–469.
- 489 Charney, J. G. and Drazin, P. G. (1961) Propagation of planetary-scale disturbances from the lower into the upper atmosphere.  
490 *Journal of Geophysical Research*, **66**, 83–109. URL: [http://onlinelibrary.wiley.com/doi/10.1029/JZ066i001p00083/](http://onlinelibrary.wiley.com/doi/10.1029/JZ066i001p00083/abstract)  
491 [abstracthttp://onlinelibrary.wiley.com/store/10.1029/JZ066i001p00083/asset/jgr2289.pdf?v=1&t=hmV2kmmz&s=](http://onlinelibrary.wiley.com/store/10.1029/JZ066i001p00083/asset/jgr2289.pdf?v=1&t=hmV2kmmz&s=0d9a140cc0c43368bd778a88ccadfc341689b634)  
492 [0d9a140cc0c43368bd778a88ccadfc341689b634](http://onlinelibrary.wiley.com/store/10.1029/JZ066i001p00083/asset/jgr2289.pdf?v=1&t=hmV2kmmz&s=0d9a140cc0c43368bd778a88ccadfc341689b634).
- 493 Cohen, J. and Jones, J. (2011) Tropospheric precursors and stratospheric warmings. *Journal of Climate*, **24**,  
494 6562–6572. URL: <http://journals.ametsoc.org/doi/pdf/10.1175/2011JCLI4160.1>  
495 [http://web.mit.edu/jlcohen/www/papers/CohenandJones\\_JC12.pdf](http://web.mit.edu/jlcohen/www/papers/CohenandJones_JC12.pdf).
- 496 Coy, L., Newman, P. A., Pawson, S. and Lait, L. R. (2017) Dynamics of the Disrupted 2015–16 Quasi-Biennial Oscillation. *Journal*  
497 *of Climate*, **30**, 5661–5674. URL: <http://dx.doi.org/10.1175/JCLI-D-16-0663.1>.

- 498 Dee, D. P., Uppala, S. M., Simmons, A. J., Berrisford, P., Poli, P., Kobayashi, S., Andrae, U., Balmaseda, M. A., Balsamo, G., Bauer,  
499 P., Bechtold, P., Beljaars, A. C. M., van de Berg, L., Bidlot, J., Bormann, N., Delsol, C., Dragani, R., Fuentes, M., Geer, A. J.,  
500 Haimberger, L., Healy, S. B., Hersbach, H., Hólm, E. V., Isaksen, I., Kållberg, P., Köhler, M., Matricardi, M., McNally, A. P.,  
501 Monge-Sanz, B. M., Morcrette, J.-J., Park, B.-K., Peubey, C., de Rosnay, P., Tavolato, C., Thépaut, J.-N. and Vitart, F. (2011)  
502 The ERA-Interim reanalysis: configuration and performance of the data assimilation system. *Quarterly Journal of the Royal*  
503 *Meteorological Society*, **137**, 553–597. URL: <http://onlinelibrary.wiley.com/doi/10.1002/qj.828/abstract>.
- 504 Deser, C., Simpson, I. R., McKinnon, K. A. and Phillips, A. S. (2017) The Northern Hemisphere extra-tropical atmospheric  
505 circulation response to ENSO: How well do we know it and how do we evaluate models accordingly? *Journal of Climate*,  
506 **30**, 5059–5082. URL: <http://dx.doi.org/10.1175/JCLI-D-16-0844.1>.
- 507 Domeisen, D. I. V., Butler, A. H., Charlton-Perez, A. J., Ayarzagüena, B., Baldwin, M. P., Dunn-Sigouin, E., Furtado, J. C.,  
508 Garfinkel, C. I., Hitchcock, P., Karpechko, A. Y., Kim, H., Knight, J., Lang, A. L., Lim, E.-P., Marshall, A., Roff, G., Schwartz,  
509 C., Simpson, I. R., Son, S.-W. and Taguchi, M. (2020a) The role of the stratosphere in subseasonal to seasonal prediction  
510 Part II: Predictability arising from stratosphere - troposphere coupling. *Journal of Geophysical Research: Atmospheres*, **125**,  
511 e2019JD030923. URL: <https://doi.org/10.1029/2019JD030923>.
- 512 – (2020b) The role of the stratosphere in subseasonal to seasonal prediction Part I: Predictability of the stratosphere. *Journal*  
513 *of Geophysical Research: Atmospheres*, **125**, e2019JD030920. URL: <https://doi.org/10.1029/2019JD030920>.
- 514 Domeisen, D. I. V., Garfinkel, C. I. and Butler, A. H. (2019) The Teleconnection of El Niño Southern Oscillation to the  
515 Stratosphere. *Reviews of Geophysics*, **57**, 5– 47. URL: <https://agupubs.onlinelibrary.wiley.com/doi/abs/10.1029/2018RG000596>.  
516
- 517 Esler, J. G. and Scott, R. K. (2005) Excitation of Transient Rossby Waves on the Stratospheric Polar Vortex and the Barotropic  
518 Sudden Warming. *Journal of the Atmospheric Sciences*, **62**, 3661–3682. URL: <https://doi.org/10.1175/JAS3557.1>.
- 519 Fletcher, C. G. and Kushner, P. J. (2013) Linear interference and the northern annular mode response to tropi-  
520 cal SST forcing: Sensitivity to model configuration. *Journal of Geophysical Research: Atmospheres*, **118**, 4267–  
521 4279. URL: [http://onlinelibrary.wiley.com/store/10.1002/jgrd.50385/asset/jgrd50385.pdf?v=1&t=hf5qrdqr&s=](http://onlinelibrary.wiley.com/store/10.1002/jgrd.50385/asset/jgrd50385.pdf?v=1&t=hf5qrdqr&s=443de1557f0ddbcabb740a81a399b5cec1dfb14f)  
522 [443de1557f0ddbcabb740a81a399b5cec1dfb14f](http://onlinelibrary.wiley.com/store/10.1002/jgrd.50385/asset/jgrd50385.pdf?v=1&t=hf5qrdqr&s=443de1557f0ddbcabb740a81a399b5cec1dfb14f).
- 523 Fraedrich, K., Pawson, S. and Wang, R. (1993) An EOF Analysis of the Vertical-Time Delay Structure of the Quasi-Biennial  
524 Oscillation. *Journal of the Atmospheric Sciences*, **50**, 3357–3365. URL: [https://doi.org/10.1175/1520-0469\(1993\)050%](https://doi.org/10.1175/1520-0469(1993)050%3C3357:AEA0TV%3E2.O.COhttp://0.0.0.2)  
525 [3C3357:AEA0TV%3E2.O.COhttp://0.0.0.2](https://doi.org/10.1175/1520-0469(1993)050%3C3357:AEA0TV%3E2.O.COhttp://0.0.0.2).
- 526 Garfinkel, C. I., Benedict, J. J. and Maloney, E. D. (2014) Impact of the MJO on the boreal winter extratropical circulation.  
527 *Geophysical Research Letters*, **41**, 6055–6062. URL: <http://dx.doi.org/10.1002/2014GL061094>.
- 528 Garfinkel, C. I., Feldstein, S. B., Waugh, D. W., Yoo, C. and Lee, S. (2012a) Observed connection between stratospheric sudden  
529 warmings and the Madden-Julian Oscillation. *Geophysical Research Letters*, **39**. URL: <http://doi.wiley.com/10.1029/2012GL053144>.  
530
- 531 Garfinkel, C. I., Hartmann, D. L. and Sassi, F. (2010) Tropospheric precursors of anomalous Northern Hemisphere stratospheric  
532 polar vortices. *Journal of Climate*, **23**, 3282–3299. URL: [http://journals.ametsoc.org/doi/pdf/10.1175/2010JCLI3010.](http://journals.ametsoc.org/doi/pdf/10.1175/2010JCLI3010.1)  
533 [1](http://journals.ametsoc.org/doi/pdf/10.1175/2010JCLI3010.1).
- 534 Garfinkel, C. I., Schwartz, C., Domeisen, D. I. V., Son, S.-W., Butler, A. H. and White, I. P. (2018) Extratropical Atmospheric  
535 Predictability From the Quasi-Biennial Oscillation in Subseasonal Forecast Models. *Journal of Geophysical Research: Atmo-*  
536 *spheres*, **123**, 7855–7866. URL: <https://agupubs.onlinelibrary.wiley.com/doi/abs/10.1029/2018JD028724>.
- 537 Garfinkel, C. I., Shaw, T. a., Hartmann, D. L. and Waugh, D. W. (2012b) Does the Holton–Tan Mechanism Explain How the  
538 Quasi-Biennial Oscillation Modulates the Arctic Polar Vortex? *Journal of the Atmospheric Sciences*, **69**, 1713–1733. URL:  
539 <http://journals.ametsoc.org/doi/abs/10.1175/JAS-D-11-0209.1>.

- 540 Gerber, E. P. and Martineau, P. (2018) Quantifying the variability of the annular modes: reanalysis uncertainty vs. sampling  
541 uncertainty. *Atmospheric Chemistry and Physics*, **18**, 17099–17117. URL: [https://www.atmos-chem-phys.net/18/17099/](https://www.atmos-chem-phys.net/18/17099/2018/)  
542 2018/.
- 543 Greening, K. and Hodgson, A. (2019) Atmospheric analysis of the cold late February and early March 2018 over the UK.  
544 *Weather*, **74**, 79–85. URL: <https://rmets.onlinelibrary.wiley.com/doi/abs/10.1002/wea.3467>.
- 545 Henderson, S. A., Maloney, E. D. and Barnes, E. A. (2016) The Influence of the Madden-Julian Oscillation on Northern Hemi-  
546 sphere Winter Blocking. *Journal of Climate*, **29**, 4597–4616. URL: [http://journals.ametsoc.org/doi/abs/10.1175/JCLI-](http://journals.ametsoc.org/doi/abs/10.1175/JCLI-D-15-0502.1)  
547 [D-15-0502.1](http://journals.ametsoc.org/doi/abs/10.1175/JCLI-D-15-0502.1).
- 548 Holton, J. R. and Tan, H.-C. (1980) The Influence of the Equatorial Quasi-Biennial Oscillation on the Global Circulation at 50  
549 mb. *Journal of the Atmospheric Sciences*, **37**, 2200–2208. URL: [http://dx.doi.org/10.1175/1520-0469\(1980\)037<2200:](http://dx.doi.org/10.1175/1520-0469(1980)037<2200:TIOTEQ>2.0.CO;2)  
550 [TIOTEQ>2.0.CO;2](http://dx.doi.org/10.1175/1520-0469(1980)037<2200:TIOTEQ>2.0.CO;2).
- 551 Hoskins, B. J. and Karoly, D. J. (1981) The Steady Linear Response of a Spherical Atmosphere to Thermal and Orographic  
552 Forcing. *Journal of the Atmospheric Sciences*, **38**, 1179–1196. URL: [http://journals.ametsoc.org/doi/abs/10.1175/1520-](http://journals.ametsoc.org/doi/abs/10.1175/1520-0469(1981)038<1179:TSLROA>2.0.CO;2)  
553 [0469\(1981\)038<1179:TSLROA>2.0.CO;2](http://journals.ametsoc.org/doi/abs/10.1175/1520-0469(1981)038<1179:TSLROA>2.0.CO;2).
- 554 Kang, W. and Tziperman, E. (2017) More frequent Sudden Stratospheric Warming events due to enhanced MJO forcing  
555 expected in a warmer climate. *Journal of Climate*, **30**, 8727–8743. URL: <https://doi.org/10.1175/JCLI-D-17-0044.1>.
- 556 Karpechko, A., Charlton-Perez, A., Balmaseda, M., Tyrrell, N. and Vitart, F. (2018) Predicting Sudden Stratospheric Warming  
557 2018 and its Climate Impacts with a Multi-Model Ensemble. *Geophysical Research Letters*, **45**, 13,538– 13,546. URL:  
558 <https://agupubs.onlinelibrary.wiley.com/doi/abs/10.1029/2018GL081091>.
- 559 Karpechko, A. Y. (2018) Predictability of Sudden Stratospheric Warmings in the ECMWF Extended-Range Forecast System.  
560 *Monthly Weather Review*, **146**, 1063–1075. URL: <https://doi.org/10.1175/MWR-D-17-0317.1>.
- 561 Karpechko, A. Y., Hitchcock, P., Peters, D. H. W. and Schneidereit, A. (2017) Predictability of downward propagation of major  
562 sudden stratospheric warmings. *Quarterly Journal of the Royal Meteorological Society*, **143**, 1459–1470. URL: [http://dx.](http://dx.doi.org/10.1002/qj.3017)  
563 [doi.org/10.1002/qj.3017](http://dx.doi.org/10.1002/qj.3017).
- 564 Lawrence, Z. D. and Manney, G. L. (2018) Characterizing Stratospheric Polar Vortex Variability With Computer Vision Tech-  
565 niques. *Journal of Geophysical Research: Atmospheres*, **123**, 1510–1535. URL: <http://dx.doi.org/10.1002/2017JD027556>.
- 566 – (2020) Does the Arctic stratospheric polar vortex exhibit signs of preconditioning prior to sudden stratospheric warmings?  
567 *Journal of the Atmospheric Sciences*, **77**, 611–632. URL: <https://doi.org/10.1175/JAS-D-19-0168.1>.
- 568 Lee, S. H. and Butler, A. H. (2019) The 2018–2019 Arctic stratospheric polar vortex. *Weather*, **75**, 52–57. URL: <https://doi.org/10.1002/wea.3643>.
- 569
- 570 Lee, S. H., Charlton-Perez, A. J., Furtado, J. C. and Woolnough, S. J. (2019) Abrupt stratospheric vortex weakening associated  
571 with North Atlantic anticyclonic wave breaking. *Journal of Geophysical Research: Atmospheres*, **124**, 8563– 8575. URL:  
572 <https://doi.org/10.1029/2019JD030940>.
- 573 Lim, Y., Son, S.-W. and Kim, D. (2018) MJO prediction skill of the subseasonal-to-seasonal prediction models. *Journal of*  
574 *Climate*, **31**, 4075–4094. URL: <https://doi.org/10.1175/JCLI-D-17-0545.1>.
- 575 Lin, H., Brunet, G. and Derome, J. (2009) An Observed Connection between the North Atlantic Oscillation and the  
576 Madden-Julian Oscillation. *Journal of Climate*, **22**, 364–380. URL: [http://journals.ametsoc.org/doi/abs/10.1175/](http://journals.ametsoc.org/doi/abs/10.1175/2008JCLI2515.1)  
577 [2008JCLI2515.1](http://journals.ametsoc.org/doi/abs/10.1175/2008JCLI2515.1).
- 578 Liu, C., Tian, B., Li, K.-F., Manney, G. L., Livesey, N. J., Yung, Y. and Waliser, D. E. (2014) Northern Hemisphere mid-winter  
579 vortex-displacement and vortex-split stratospheric sudden warmings: Influence of the Madden-Julian Oscillation and  
580 Quasi-Biennial Oscillation. *Journal of Geophysical Research: Atmospheres*, 2014JD021876. URL: [http://dx.doi.org/10.](http://dx.doi.org/10.1002/2014JD021876)  
581 [1002/2014JD021876](http://dx.doi.org/10.1002/2014JD021876).

- 582 Lu, H., Hitchman, M. H., Gray, L. J., Anstey, J. A. and Osprey, S. M. (2020) On the Role of Rossby Wave Breaking in the Quasi-  
583 Biennial Modulation of the Stratospheric Polar Vortex during Boreal Winter. *Quarterly Journal of the Royal Meteorological*  
584 *Society*, 1– 21. URL: <https://doi.org/10.1002/qj.3775>.
- 585 Martius, O., Polvani, L. M. and Davies, H. C. (2009) Blocking precursors to stratospheric sudden warming events. *Geophysical*  
586 *Research Letters*, **36**, L14806. URL: <http://doi.wiley.com/10.1029/2009GL038776>.
- 587 Matthewman, N. J., Esler, J. G., Charlton-Perez, A. J. and Polvani, L. M. (2009) A New Look at Stratospheric Sudden Warmings.  
588 Part III: Polar Vortex Evolution and Vertical Structure. *Journal of Climate*, **22**, 1566–1585. URL: <http://journals.ametsoc.org/doi/abs/10.1175/2008JCLI2365.1>.
- 590 Mitchell, D. M., Gray, L. J., Anstey, J., Baldwin, M. P. and Charlton-Perez, A. J. (2013) The Influence of Stratospheric Vortex  
591 Displacements and Splits on Surface Climate. *Journal of Climate*, **26**, 2668–2682. URL: <http://journals.ametsoc.org/doi/abs/10.1175/JCLI-D-12-00030.1>.
- 593 Peings, Y. (2019) Ural Blocking as a driver of early winter stratospheric warmings. *Geophysical Research Letters*, **46**, 5460–  
594 5468. URL: <https://agupubs.onlinelibrary.wiley.com/doi/abs/10.1029/2019GL082097>.
- 595 Rao, J., Garfinkel, C. I., Chen, H. and White, I. P. (2019) The 2019 New Year Stratospheric Sudden Warming and Its Real-Time  
596 Predictions in Multiple S2S Models. *Journal of Geophysical Research: Atmospheres*, **124**. URL: <https://doi.org/10.1029/2019JD030826>.
- 598 Rao, J., Garfinkel, C. I. and White, I. P. (2020) Predicting the Downward and Surface Influence of the February 2018 and  
599 January 2019 Sudden Stratospheric Warming Events in Subseasonal to Seasonal (S2S) Models. *Journal of Geophysical*  
600 *Research: Atmospheres*, **125**, e2019JD031919. URL: <https://doi.org/10.1029/2019JD031919>.
- 601 Rao, J., Ren, R., Chen, H., Yu, Y. and Zhou, Y. (2018) The Stratospheric Sudden Warming Event in February 2018 and its  
602 Prediction by a Climate System Model. *Journal of Geophysical Research: Atmospheres*, **123**, 313–332. URL: <https://agupubs.onlinelibrary.wiley.com/doi/abs/10.1029/2018JD028908>.
- 604 Rashid, H. A., Hendon, H. H., Wheeler, M. C. and Alves, O. (2011) Prediction of the Madden–Julian oscillation with the POAMA  
605 dynamical prediction system. *Climate Dynamics*, **36**, 649–661. URL: <https://doi.org/10.1007/s00382-010-0754-x>.
- 606 Saha, S., Moorthi, S., Wu, X., Wang, J., Nadiga, S., Tripp, P., Behringer, D., Hou, Y.-T., Chuang, H.-y., Iredell, M., Ek, M., Meng,  
607 J., Yang, R., Peña Mendez, M., van den Dool, H., Zhang, Q., Wang, W., Chen, M. and Becker, E. (2014) The NCEP Climate  
608 Forecast System Version 2. *Journal of Climate*, **27**, 2185–2208. URL: <http://journals.ametsoc.org/doi/abs/10.1175/JCLI-D-12-00823.1?af=R>.
- 610 Seviour, W. J. M., Mitchell, D. M. and Gray, L. J. (2013) A practical method to identify displaced and split stratospheric polar  
611 vortex events. *Geophysical Research Letters*, **40**, 5268–5273. URL: <http://onlinelibrary.wiley.com/doi/10.1002/grl.50927/abstract>.
- 613 Shi, C., Xu, T., Guo, D. and Pan, Z. (2017) Modulating Effects of Planetary Wave 3 on a Stratospheric Sudden Warming Event  
614 in 2005. *Journal of the Atmospheric Sciences*, **74**, 1549–1559. URL: <https://doi.org/10.1175/JAS-D-16-0065.1>.
- 615 Smith, A. K. (1983) Observation of Wave-Wave Interactions in the Stratosphere. *Journal of the Atmospheric Sciences*, **40**,  
616 2484–2496. URL: [https://doi.org/10.1175/1520-0469\(1983\)040%3C2484:00WII%3E2.0.COhttp://0.0.0.2](https://doi.org/10.1175/1520-0469(1983)040%3C2484:00WII%3E2.0.COhttp://0.0.0.2).
- 617 Smith, K. L. and Kushner, P. J. (2012) Linear interference and the initiation of extratropical stratosphere-troposphere interac-  
618 tions. *Journal of Geophysical Research-Atmospheres*, **117**.
- 619 Taguchi, M. (2015) Connection of predictability of major stratospheric sudden warmings to polar vortex geometry. *Atmospheric*  
620 *Science Letters*, **17**, 33–38. URL: <http://dx.doi.org/10.1002/asl.595>.
- 621 – (2018) Comparison of Subseasonal-to-Seasonal Model Forecasts for Major Stratospheric Sudden Warmings. *Journal of*  
622 *Geophysical Research: Atmospheres*, **123**, 210–231. URL: <https://agupubs.onlinelibrary.wiley.com/doi/abs/10.1029/2018JD028755>.
- 623

- 624 Tripathi, O. P., Baldwin, M., Charlton-Perez, A., Charron, M., Eckermann, S. D., Gerber, E., Harrison, R. G., Jackson, D. R., Kim,  
625 B.-M., Kuroda, Y., Lang, A., Mahmood, S., Mizuta, R., Roff, G., Sigmond, M. and Son, S.-W. (2014) The predictability of the  
626 extratropical stratosphere on monthly time-scales and its impact on the skill of tropospheric forecasts. *Quarterly Journal*  
627 *of the Royal Meteorological Society*, 987–1003. URL: <http://dx.doi.org/10.1002/qj.2432>.
- 628 Vitart, F. (2017) Madden-Julian Oscillation Prediction and Teleconnections in the S2S Database. *Quarterly Journal of the Royal*  
629 *Meteorological Society*, **143**, 2210–2220. URL: <http://dx.doi.org/10.1002/qj.3079>.
- 630 Vitart, F., Ardilouze, C., Bonet, A., Brookshaw, A., Chen, M., Codorean, C., Déqué, M., Ferranti, L., Fucile, E., Fuentes, M., Hen-  
631 don, H., Hodgson, J., Kang, H. S., Kumar, A., Lin, H., Liu, G., Liu, X., Malguzzi, P., Mallas, I., Manoussakis, M., Mastrangelo,  
632 D., MacLachlan, C., McLean, P., Minami, A., Mladek, R., Nakazawa, T., Najm, S., Nie, Y., Rixen, M., Robertson, A. W., Ruti, P.,  
633 Sun, C., Takaya, Y., Tolstykh, M., Venuti, F., Waliser, D., Woolnough, S., Wu, T., Won, D.-J., Xiao, H., Zaripov, R. and Zhang,  
634 L. (2017) The Sub-seasonal to Seasonal Prediction (S2S) Project Database. *Bulletin of the American Meteorological Society*,  
635 **98**, 162–173. URL: <http://dx.doi.org/10.1175/BAMS-D-16-0017.1>.
- 636 Wang, R., Fraedrich, K. and Pawson, S. (1995) Phase-Space Characteristics of the Tropical Stratospheric Quasi-Biennial Oscil-  
637 lation. *Journal of the Atmospheric Sciences*, **52**, 4482–4500. URL: [https://doi.org/10.1175/1520-0469\(1995\)052%3C4482:](https://doi.org/10.1175/1520-0469(1995)052%3C4482:PCOTTS%3E2.0.CO;2)  
638 [PCOTTS%3E2.0.CO;2](https://doi.org/10.1175/1520-0469(1995)052%3C4482:PCOTTS%3E2.0.CO;2)<http://0.0.0.2>.
- 639 Wheeler, M. C. and Hendon, H. H. (2004) An All-Season Real-Time Multivariate MJO Index: Development of an Index for  
640 Monitoring and Prediction. *Monthly Weather Review*, **132**, 1917–1932. URL: [https://doi.org/10.1175/1520-0493\(2004\)](https://doi.org/10.1175/1520-0493(2004)132%3C1917:AARMMI%3E2.0.CO;2)  
641 [132%3C1917:AARMMI%3E2.0.CO;2](https://doi.org/10.1175/1520-0493(2004)132%3C1917:AARMMI%3E2.0.CO;2)<http://0.0.0.2>.
- 642 White, I., Garfinkel, C. I., Gerber, E. P., Jucker, M., Aquila, V. and Oman, L. D. (2019) The Downward Influence of Sudden  
643 Stratospheric Warmings: Association with Tropospheric Precursors. *Journal of Climate*, **32**, 85–108. URL: [https://doi.](https://doi.org/10.1175/JCLI-D-18-0053.1)  
644 [org/10.1175/JCLI-D-18-0053.1](https://doi.org/10.1175/JCLI-D-18-0053.1).
- 645 White, I. P., Lu, H., Mitchell, N. J. and Phillips, T. (2015) Dynamical Response to the QBO in the Northern Winter Stratosphere:  
646 Signatures in Wave Forcing and Eddy Fluxes of Potential Vorticity. *Journal of the Atmospheric Sciences*, **72**, 4487–4507.  
647 URL: <http://dx.doi.org/10.1175/JAS-D-14-0358.1>.
- 648 Woollings, T., Charlton-Perez, A., Ineson, S., Marshall, A. G. and Masato, G. (2010) Associations between stratospheric vari-  
649 ability and tropospheric blocking. *Journal of Geophysical Research: Atmospheres*, **115**. URL: [https://doi.org/10.1029/](https://doi.org/10.1029/2009JD012742)  
650 [2009JD012742](https://doi.org/10.1029/2009JD012742).

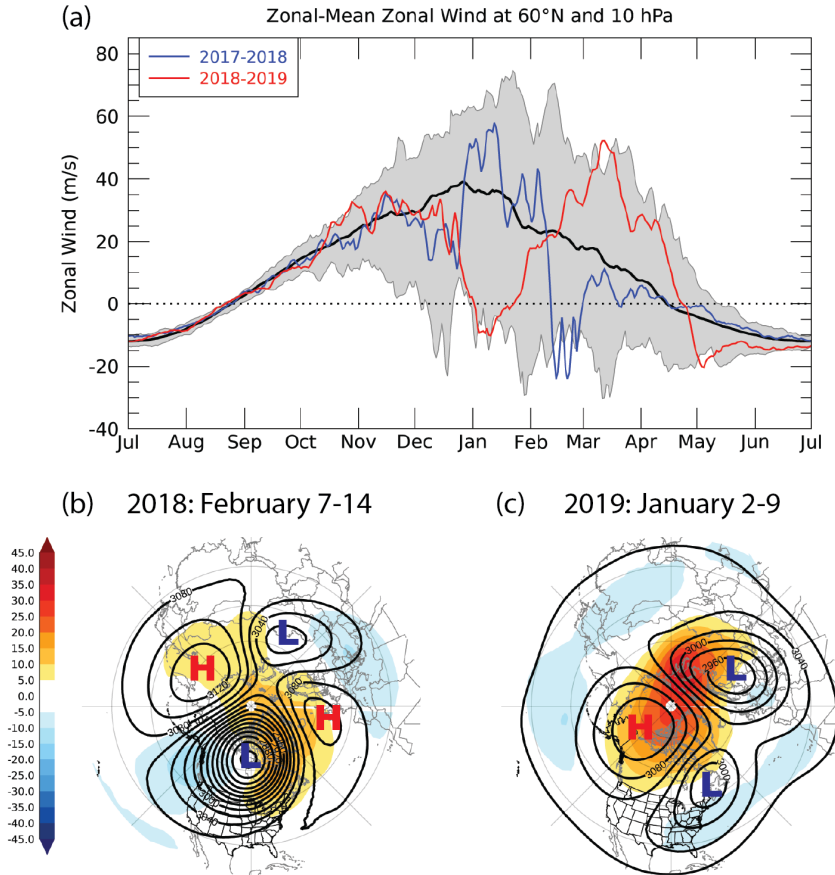


**FIGURE 1** (a) Time series of the ERA-Interim 10 hPa 60°N zonal-mean zonal winds for 2017-2018 (blue line) and 2018-2019 (red line) overlying the daily mean (black line) and daily maximum and minimum (grey shading). The daily statistics are based on the 1979-2017 record. Averaged 10 hPa geopotential heights [dam] (contour) and 10 hPa temperature anomalies [K] (shading) for the (b) 7-14 February 2018, and the (c) 2-9 January 2019 period.

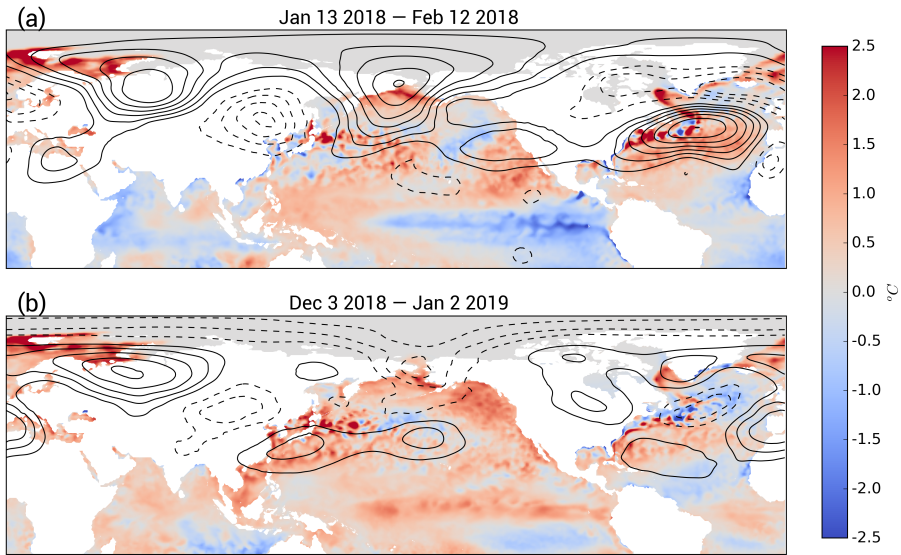


**FIGURE 2** Sea surface temperature anomalies (shading, [degrees C]) and 500 hPa geopotential height anomalies (contoured every 30 m, omitting the 0 contour) from ERA-interim for 30 days preceding the vortex split on (a) 12 February 2018 and (b) 2 January 2019.

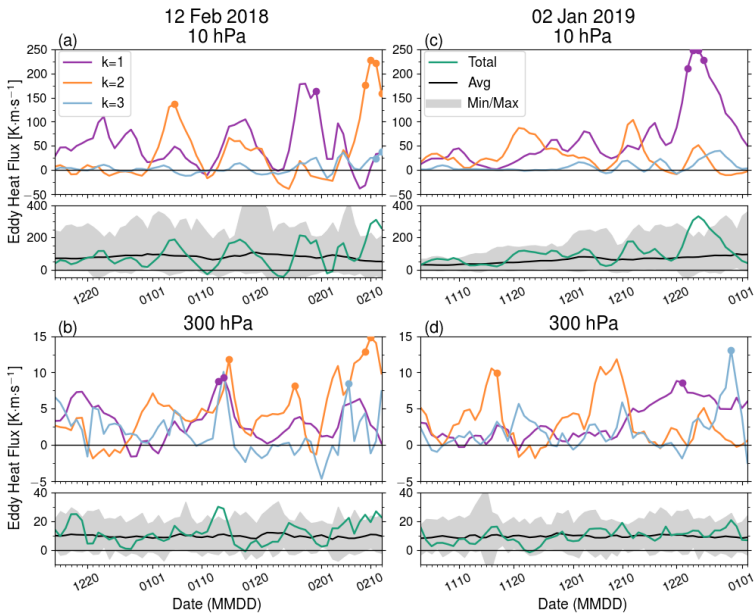


**FIGURE 3** Time series of 40-80°N averaged eddy heat flux due to wavenumbers  $k=1$ , 2, and 3 on top of total eddy heat fluxes (green line) and their daily climatological extremes for the 1979-2017 period (gray shading) for 60 days before (a,b) the 2018 event and (c,d) the 2019 event, for (a,c) 10 hPa and (b,d) 300 hPa. Times when the wave-component heat fluxes are maxima in the ERA-Interim record are denoted with dots.

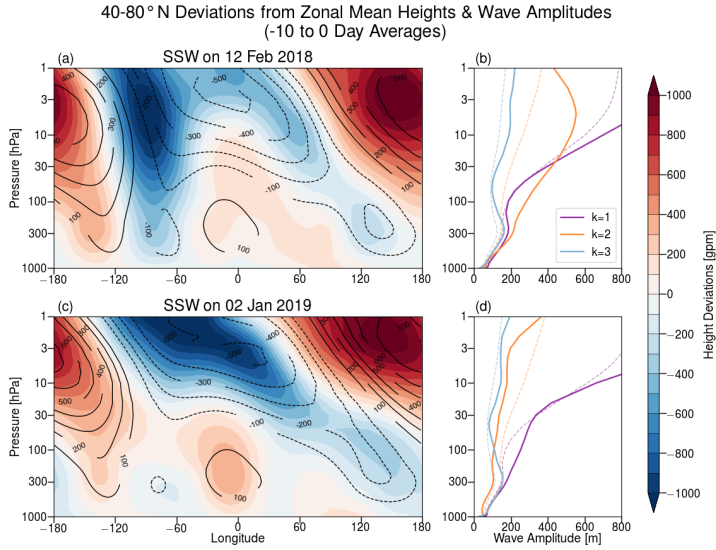


**FIGURE 4** (a,c) Longitude by height cross-sections of 40-80°N deviations from zonal mean geopotential heights, and (b,d) the corresponding wave amplitudes for wavenumbers  $k=1-3$ , composited over days -10 to 0 prior to the (a,b) 2018 SSW and (c,d) 2019 SSW. In (a,c), the climatological height deviations from zonal mean for the same days are shown by black contours. In (b,d) the climatological wave amplitudes are shown by light dashed lines.

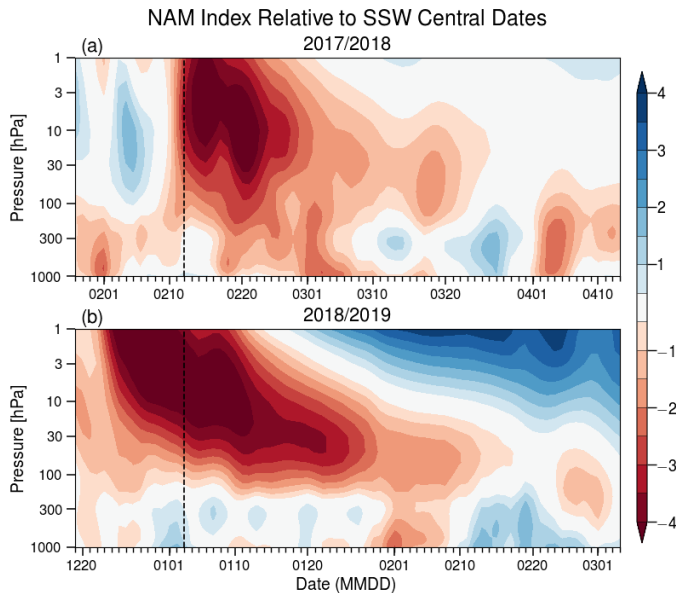


**FIGURE 5** Time series of the Northern Annular Mode index as a function of pressure, for 15 days before and 60 days following the (a) 12 February 2018 and (b) 2 January 2019 sudden warming events.

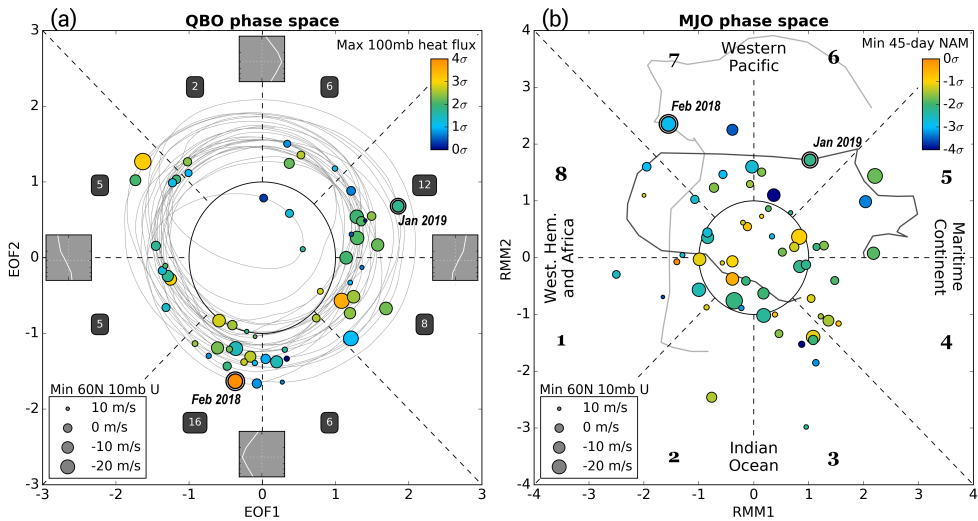


**FIGURE 6** a) QBO phase space, with grey lines tracing the historical QBO and colored dots representing vortex weakening events (using ERA-40 reanalysis from 1960-1979, ERA-Interim from 1979-2019). The marker size corresponds to the magnitude of zonal-mean zonal wind reversal at 10 hPa and 60°N, and the color corresponds to the maximum 100 hPa 45-75°N eddy heat flux anomaly in the 10 days prior to each vortex event. For visualization, the grey box every 90 degrees shows the vertical profile of tropical (5°S-5°N) zonal-mean zonal winds, as a function of pressure, for that location in phase space. The horizontal white dashed line in the box represents 30 hPa. The number of vortex weakening events in each octant of the QBO phase space is provided in a dark grey box. b) State of the RMM index for the two events as compared with vortex weakening events since 1979 (based on ERA-Interim only), with the marker size corresponding to intensity and the color corresponding to the minimum 1000 hPa NAM value in the 45 days following the vortex events. Gray lines trace the MJO for 15 days prior to 15 days after the 12 February 2018 SSW (light gray) and 2 January 2019 SSW (dark gray).

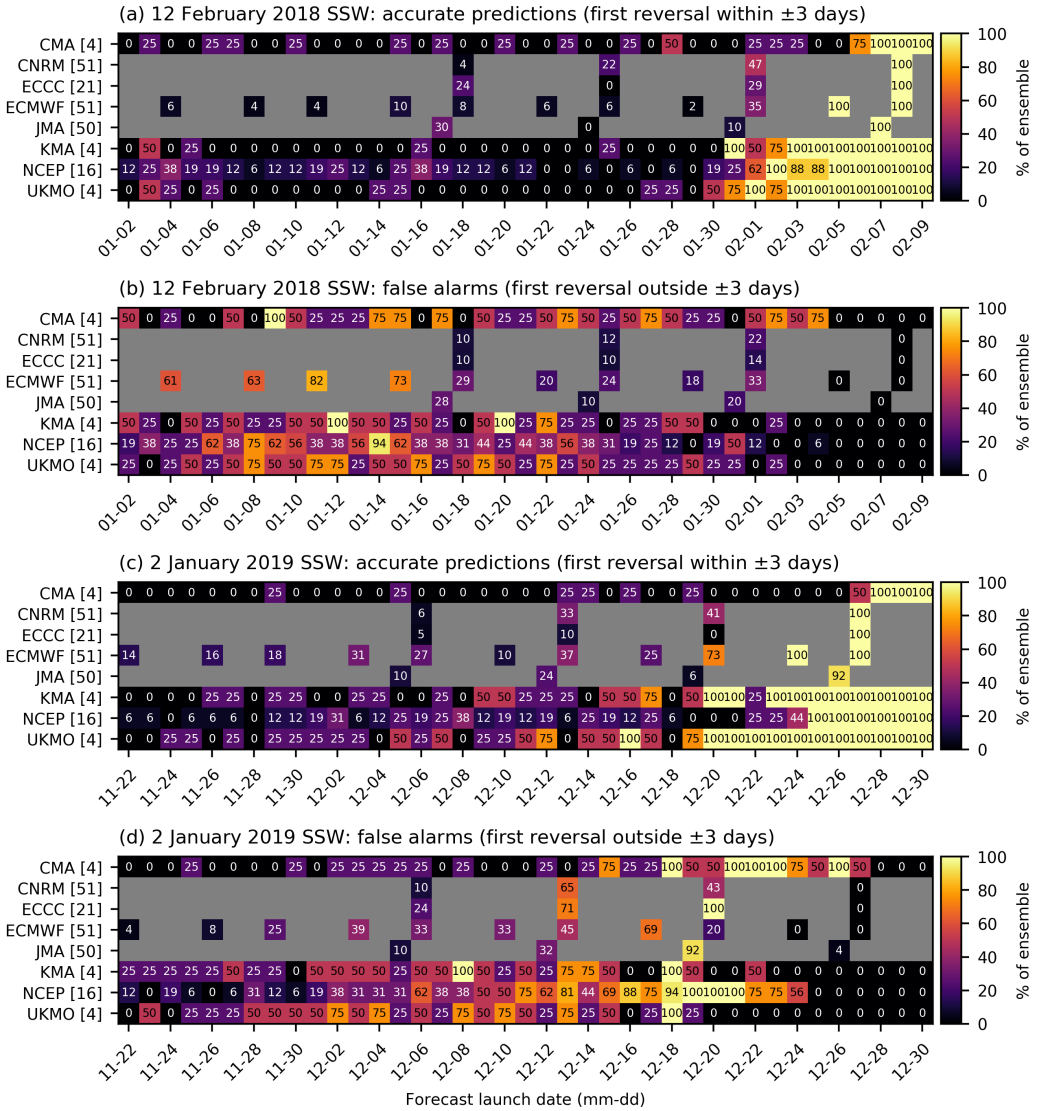


**FIGURE 7** Percent of bias-corrected ensemble members from prediction systems participating in the S2S database that (a,c) correctly detected the first zonal wind reversal at 10 hPa and 60°N within  $\pm 3$  days of the observed event, and (b,d) detected the first zonal wind reversal at 10 hPa and 60°N outside the  $\pm 3$  day window, for the (a,b) 2018 SSW and the (c,d) 2019 SSW.

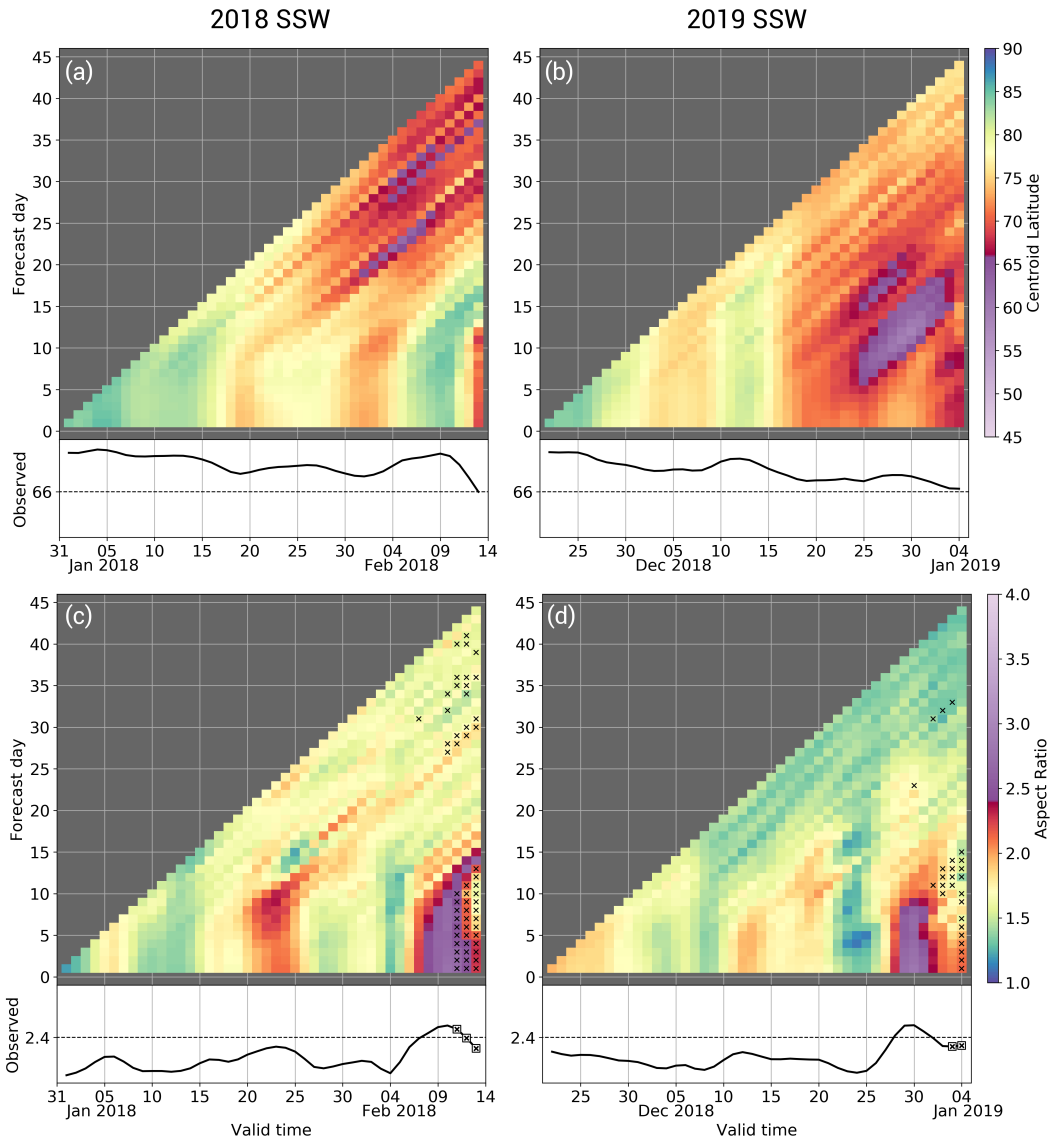


**FIGURE 8** NCEP CFSv2 forecasts, as a function of initialization date (x-axis) and forecast day (y-axis), of (a,b) the vortex centroid latitude and (c,d) the aspect ratio, for the (a,c) 2018 SSW and the (b,d) 2019 SSW. The ERA-Interim moment diagnostics for each day are shown beneath each chiclet plot. The vortex can be said to be “displaced” when the centroid latitude is less than 66 degrees latitude, and to be “split” when the aspect ratio is greater than 2.4. The x’s indicate where a region segmentation algorithm detected more than 1 distinct vortex region in ERA-Interim, or where the algorithm detected splits in more than half of the CFSv2 ensemble members.

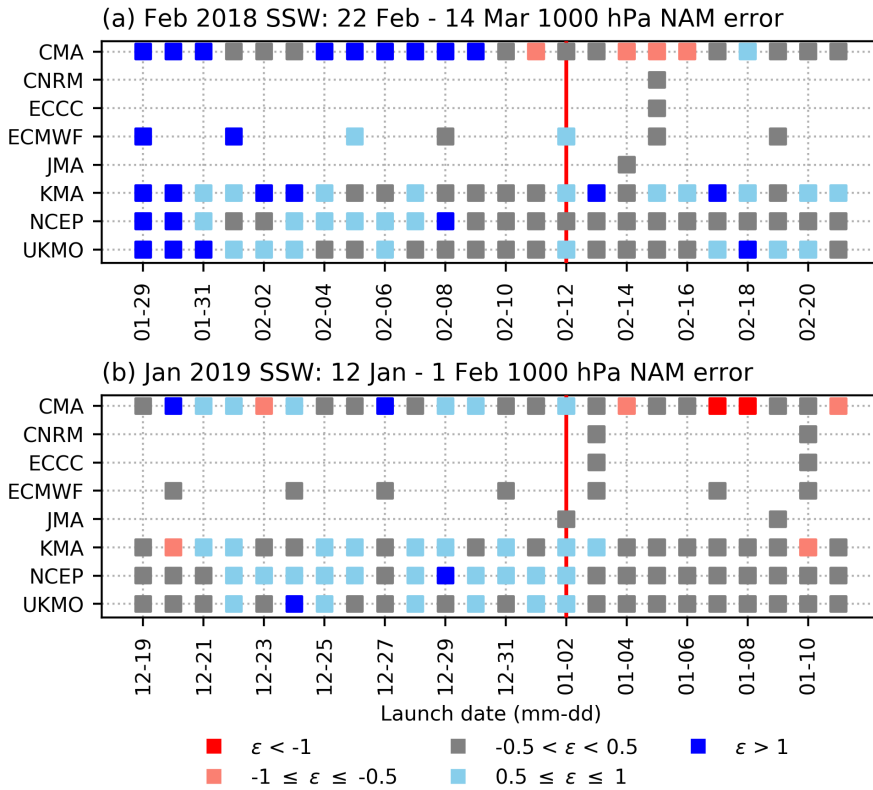


**FIGURE 9** Difference between S2S ensemble mean forecasts for the average 1000 hPa NAM for 10-30 days following the 2018 and 2019 SSWs and verification from ERA-Interim. In (a) this is for the period 22 February–14 March, in (b) this is 12 January–1 February. Gray indicates the magnitude of the difference to the observed value was  $<0.5$ , light red (light blue) indicates the forecast NAM was 0.5–1.0 standard deviations more negative (positive) than verification, and red (blue) indicates this difference exceeded 1 standard deviation. The vertical red line in each panel indicates the date of the SSW.

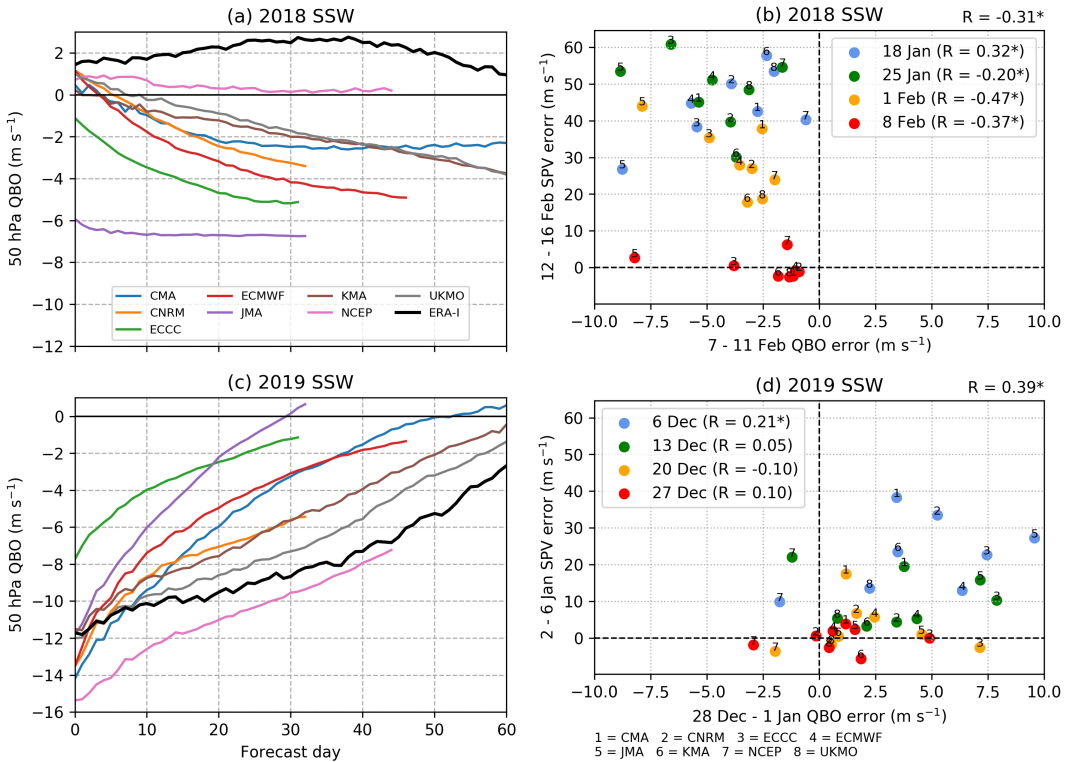


**FIGURE 10** Tropical zonal-mean zonal winds averaged from 5°N-5°S at 50 hPa prior to (a) 2018 SSW and (b) 2019 SSW. These values are created by averaging forecasts over 4 launch dates consistent across prediction systems: 18 Jan, 25 Jan, 1 Feb, and 8 Feb 2018; and 6 Dec, 13 Dec, 20 Dec, and 27 Dec 2018 (note: JMA launches a day earlier). The black-line is ERA-Interim sub-sampled and averaged in an identical manner. Scatterplots of the averaged error in the QBO forecasts versus error in the zonal-mean zonal winds at 60°N and 10 hPa (SPV), for (b) 2018: QBO 7-11 Feb (8-11 Feb for 8 Feb launch date, except ECCC 9-11 Feb), SPV 12-16 Feb, and (d) 2019: QBO 28 Dec-1 Jan, SPV 2-6 Jan [i.e. 5 days before/after SSW]. Correlation values are calculated using the multi-model ensemble of 201 members. Only ensemble-mean values are shown. In all panels, these are hindcast bias-corrected. An asterisk indicates the correlation is significant at the 95% confidence level according to a bootstrap re-sampling test (10,000 repeats).

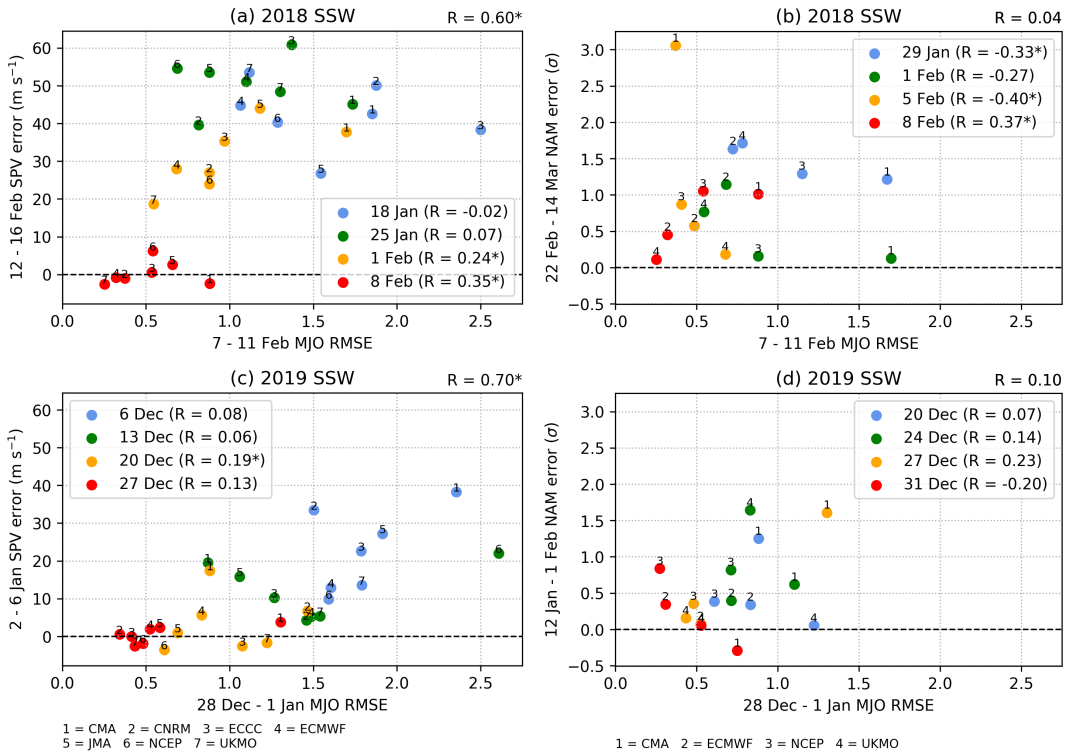


**FIGURE 11** Scatterplots of the averaged bivariate RMSE in the MJO forecasts for the 5 days before each SSW [(a, b) 7 - 11 Feb (8 - 11 Feb for 8 Feb launch date except ECCS 9 - 11 Feb), (c, d) 28 Dec - 1 Jan] versus (a, c) error in the zonal-mean zonal winds at  $60^\circ\text{N}$  and 10 hPa (SPV) 5 days after the SSW and (b, d) error in the 1000 hPa NAM 10-30 days after the SSW (as in Figure 9). Correlation values are calculated using the multi-model ensemble of (a,c) 201 and (b,d) 75 members. Only ensemble-mean values are shown. In all panels, these are hindcast bias corrected. An asterisk indicates the correlation is significant at the 95% confidence level according to a bootstrap re-sampling test (10,000 repeats).